Supplemental Material to: Sum-Frequency Generation at Molecule-Nanostructure Interfaces from Diagrammatic Theory of Nonlinear Optics

T. Noblet · B. Busson

Contents

1 Differences between the Matsubara formalism and its optical formulation **2**
1.1 General discussion . . . 2
1.2 Differences in filling the Feynman diagrams . . . 2
1.3 Differences in calculating the Feynman diagrams . . . 3
1.4 Feynman rules for nonlinear optics . . . 4

2 Mathematical origin of modified Feynman rules for optics **5**
2.1 Rule #11: Analytical continuity of Green's functions . . . 5
2.2 Rule #8: Signature of optical loop diagrams . . . 5
2.3 Rule #8: Counting of internal Matsubara frequencies . . . 6
2.4 Rule #5: Matsubara frequencies of virtual bosons . . . 7
2.5 Rule #9: Summations over quantum states and Matsubara frequencies . . . 8

3 Canonical linear and nonlinear optical response functions **10**
3.1 First-order polarizability . . . 10
3.2 Second-order hyperpolarizability . . . 10
3.3 Third-order hyperpolarizability . . . 11
3.4 Fifth-order hyperpolarizability . . . 11

4 Factorization of odd-order response functions **12**
4.1 Factorization of third-order functions $\boldsymbol{\gamma_{ijkl}}$ . . . 12
4.2 Factorization of fifth-order functions $\boldsymbol{\xi_{ijkluv}}$ . . . 14
4.3 Generalization . . . 15

5 Pairing of diagrams **16**
5.1 One-boson diagrams ($V = 1$) . . . 16
5.2 Two-boson diagrams ($V = 2$) . . . 17
5.3 Three-boson diagrams ($V = 3$) . . . 19

1 Differences between the Matsubara formalism and its optical formulation

1.1 General discussion

The Green-Matsubara formalism was originally developed to handle N-particle interactions within solids at an arbitrary temperature. It allows to express quantum Green's functions for solid-state physics in the frequency domain through a perturbative expansion as a function of a growing number of interaction processes, whose orders are easily represented by Feynman loop-diagrams. In a previous paper [1], we have shown that the formalism could be adapted in order to compute the linear and nonlinear optical responses of a system composed of several interacting entities, as optical response functions belong to Green's functions. Here we would like to elaborate on the differences between the original Green-Matsubara formalism and its optical formulation.

In the original Green-Matsubara formalism, all frequencies (associated to both fermion and boson states) appearing in a Feynman diagram are Matsubara frequencies (as defined in Part 2.1): input and output frequencies; frequencies propagating inside a loop; virtual bosons associated with interaction processes. The Feynman diagram is then computed by summing over all the internal Matsubara frequencies and considering all the possible values for the input and output frequencies.

In the optical formalism, there are substantial differences in the constraints put on the system:

1. the input and output frequencies of the response functions, representing photons getting in and out of the system, are fixed and freely chosen by the experimenter;

2. each interaction process is fully described by an interaction hamiltonian which is exactly known; the associated coupling constants are not supposed weak and, consequently, Feynman diagrams at all orders have to be included in the calculation (it does not consist in a perturbative expansion);

3. diagrams represent composite systems made of several sub-units (e.g. a molecule and the nanoparticle on which it is adsorbed) so that each loop embodies a given sub-unit, thus described as an N-particle system interacting with the other(s); these sub-units can either be an assembly of N identical particles (like in a solid-state description), or the distribution of N discrete eigenstates of an entity (e.g. a molecule) defined by a constitutive hamiltonian; this is quite different from the classical formalism wherein all the loops of a diagram represent the propagation of different states of the same N-particle system;

4. the interactions take place between these defined and separated sub-units, and proceed from optical processes; as a consequence, the virtual bosons exchanged within the diagrams actually represent real vector bosons (i.e. photons).

Point #3 has been addressed in Ref. [1]. A correspondence between the fermion distribution function $\rho(\omega_m)$ and the density matrix diagonal elements $\hat{\rho}_{mm}$ allows to treat either condensed matter or discrete eigenstate entities by means of the same formalism. These four differences translate into an adaptation of the original Feynman rules, governing the drawing and the calculation of the Feynman diagrams, into new ones (recalled in Part 1.4) adapted to the optical response functions.

The description introduced in Ref. [1] implicitly integrates these differences, but we detail them here in order to establish a firm link between classical and optical formulations, ensuring the rigor of the latter while clarifying its specific hypotheses and implicit assumptions.

1.2 Differences in filling the Feynman diagrams

In Figure S1, we illustrate the two ways (classical and optical) to draw and fill a Feynman diagram. On the right, we recognize diagram [2,1,↓↑] as sketched in the main text of the present paper (Figure 2). On the left, the same diagram is shown with all frequencies defined according to the classical Matsubara formalism. The differences are twofold: first, the input and output frequencies in the classical diagram belong to Matsubara frequencies (leading to the calculation of $\tilde{\beta}(\imath\omega_\eta, \imath\omega_\kappa)$, where $\tilde{\beta}$ defines the hyperpolarizability in the Matsubara frequency space), whereas $\imath\omega_1$ and $\imath\omega_2$ ($\imath\omega_3 = \imath\omega_1 + \imath\omega_2$) are arbitrarily chosen in the optical diagram for the definition of $\tilde{\beta}(\imath\omega_1, \imath\omega_2)$. In order to understand this point, we have to get back to the mathematical foundations of the Green-Matsubara approach, which are briefly recalled in Part 2.1. This summary shows that all frequencies involved in a Feynman diagram must indeed be Matsubara frequencies, i.e. a multiple of $\pi/\hbar b$, over which a summation is performed

to compute the diagram, before implementing analytical continuity to recover the response functions expressed in real frequencies. This is not strictly fulfilled in the optical diagrams. Choosing at will the input and output frequencies implies that the set of Matsubara frequencies $\imath\omega_\eta$ and $\imath\omega_\kappa$ has to continuously pave the imaginary axis in the complex plane, which is only valid when $b \to \infty$, that is for a temperature $T \to 0$. The vanishing temperature limit is therefore an implicit hypothesis of the optical formalism.

The second difference belongs to the same kind: in the optical formalism, the frequencies of the virtual bosons exchanged during interaction processes between the two loops (i.e. the two subsystems) are limited to the frequencies injected or created in the diagram (as stated by Feynman rule #5). In the classical description, these processes remain internal to the N-particle system and, as such, they also convey arbitrary Matsubara frequencies $\imath\omega_\alpha$ associated to the inner loop, over which a summation is performed. In the optical description, the subsystems are split and identified, so that the interaction takes place in a real (not virtual) sense between them. In these conditions, the bosons exchanged between the entities are not virtual anymore but become real vector bosons. Depending on the nature of the interaction, their frequencies may freely span the whole Matsubara set or be restricted to specific frequencies. Here we have focused on optical interactions in a broad sense, relying on the interplay between electric and magnetic fields on one side, electric and magnetic dipoles (and multipoles) on the other side. Consequently, only frequencies related to the oscillation of a dipole in the system may be conveyed by the interaction bosons (i.e. photons). On the one side, the hypothesis of $T \to 0$, allowing to consider all frequencies as Matsubara frequencies, makes this possible, as it is the case for the input frequencies; on the other side, it implies that the additional Matsubara frequency $\imath\omega_\alpha$ in Figure S1 has to vanish (corresponding to Feynman rule #5), leading to a separation between the loops in the Matsubara sums. This, of course, modifies the way the diagrams are calculated.

1.3 Differences in calculating the Feynman diagrams

The Feynman rules also provide a guide for calculating the diagrams in the optical formalism. From the previous paragraph, we understand that the sum over internal frequency $\imath\omega_\alpha$ is weighted by a $\delta_{\alpha,0}$ factor to fulfill rule #5 (see Part 2.4). In fact, the rules listed in Part 1.4 already integrate the disappearance of $\imath\omega_\alpha$. However, each sum over Matsubara frequencies being weighted by a factor $1/b$, like in Eq. (3), the $1/b$ related to the sum over $\imath\omega_\alpha$ remains in the overall b exponent as defined in rule #8. This has major consequences on the factorization procedure as detailed in Part 4. The counting of these factors $1/b$ in the general case is detailed in Part 2.3.

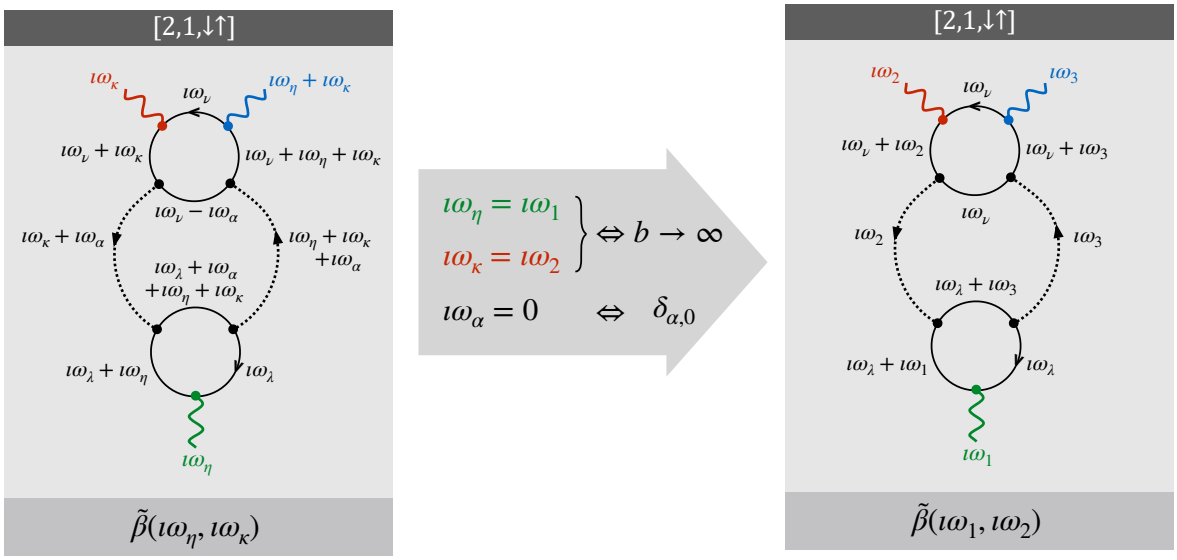

Figure S1: **Correspondence between the classical and optical formalisms.** Frequency filling of the Feynman diagram $[2, 1, \downarrow\uparrow]$ before (left) and after (right) applying the Feynman rules adapted for the computation of optical response functions. Computing optical response functions from loop diagrams in the Matsubara frequency space involves eliminating the internal boson frequencies (e.g. $\imath\omega_\alpha$) and taking the limit $b \to \infty$, i.e. $T \to 0$.

Furthermore, as explained above, the vanishing of $\imath\omega_\alpha$ stems from the nature of the interaction hamiltonian, which has a second consequence on the calculation process. This hamiltonian being related to a real (not virtual) energy exchange between the subsystems, it relates to the same order of magnitude as the fundamental process (e.g. $\tilde{\beta}^{(123)}(\imath\omega_1, \imath\omega_2)$ in the case of Figure S1). In condensed matter processes, all interactions remain internal to the N-particle system by exchange of virtual bosons, leading to their perturbative treatment: a diagram made of n virtual bosons (associated to the coupling constant W) thus represents a perturbative contribution of order n, i.e. depending on W^n. In our optical approach, diagram evaluation must take into account all the allowed orders describing a process involving the interactions, whatever the number of vector bosons (i.e. photons) exchanged. This what is done in the main text, leading to a final description of the hyperpolarizability of the molecule/nanoparticle system as a sum of all $V = 0$ to $V = 3$ processes. In essence, in optics, a perturbative expansion of the dipole moments is indeed performed with respect to the electric field (see Part 2.2), instead of a perturbative expansion with respect to the coupling constants.

1.4 Feynman rules for nonlinear optics

The extrapolation of the Feynman-Matsubara formalism from condensed matter physics to optics is based on the application of twelve rules. Here we recall them:

1) Define the system by its number N_l of partners (or subsystems); define the optical process by the number N_p of photons involved, their nature (creation or annihilation) and their frequency relationships (e.g. $\omega_3 = \omega_1 + \omega_2$ for SFG); first-order $\boldsymbol{\alpha}$ functions are represented by diagrams for which $N_p = 2$, second-order $\boldsymbol{\beta}$ functions when $N_p = 3$, and third-order $\boldsymbol{\gamma}$ functions when $N_p = 4$; indeed, in virtue of nonlinear optics theory, we know that any n^{th} order process consists in a $(n + 1)$-wave mixing, i.e. $N_p = n + 1$;

2) Define the total number N_v of interaction processes, first, between the partners and the photons (N_p) and, second, between the partners themselves ($N_v - N_p$), reminding that two nodes linked by a virtual boson propagator represent one interaction process;

3) Draw all the topologically distinct loop diagrams made of N_l loops (as many as subsystems) and N_v interaction processes;

4) For each loop, assign an implicit Matsubara frequency (e.g. $\imath\omega_\nu$) to the propagator associated to the initial state;

5) Apply the energy conservation rule (in terms of frequencies) at each vertex with boson frequencies chosen among those present in the system, by ensuring that the constitutive energy relationship (e.g. $\omega_3 = \omega_1 + \omega_2$) applies at one and only one vertex; draw as many distinct diagrams as possible by considering all allowed frequencies, initial states and directions of rotation on the loops; if some diagrams are equivalent, keep only one of them;

6) Determine for each vertex the coupling constant corresponding to the interaction hamiltonian (e.g. p^i_{nm} for light-matter interaction) and multiply them;

7) Determine for each propagator the associated imaginary-time Green's function and multiply them;

8) Multiply by $(-1)^{N_p+1} \cdot b^{N_p-N_v-1} \cdot \hbar^{N_p-2N_v}$, where $b = 1/k_BT$;

9) Sum over all the quantum numbers and all the implicit Matsubara frequencies to get the response function with imaginary frequency arguments;

10) Use the residue theorem in order to reduce the sums over the implicit frequencies;

11) Replace the imaginary frequencies $\imath\omega$ of photons by $\omega + \imath 0^+$ to get the response function with real frequency arguments;

12) Introduce the damping constants Γ_{nm} by replacing each term $(\pm\omega_{nm}+\imath 0^+)$ by $(\pm\omega_{nm}+\imath\Gamma_{nm})$. This last rule takes into account the finite lifetimes of real quantum states. Experimentally, the system is not strictly isolated (or else we could not interact with it nor characterize it), and the resonances identified through spectroscopy measurements are not ideal eigenstates. The phenomenological damping constants Γ_{nm} are added to account for the real homogeneous broadening of the theoretical eigenstates (arising from Heisenberg principle).

In order to demonstrate some results presented in the Article, we must elaborate on the mathematical origin of rules #5, #8 and #11.

2 Mathematical origin of modified Feynman rules for optics

2.1 Rule #11: Analytical continuity of Green's functions

In solid-state physics, the propagation of quantum states after excitation of the system is physically described by retarded Green's functions $G_{nm}(t)$ defined with respect to the physical time t:

$$G_{nm}(t) = -\imath\theta(t)\,\mathrm{tr}\left(\hat{\rho}^{(0)}\{c_n(t), c_m^\dagger(0)\}\right), \quad \text{with} \quad c_i(t) = e^{\imath\mathcal{H}_0 t/\hbar}\, c_i\, e^{-\imath\mathcal{H}_0 t/\hbar}. \tag{1}$$

Mathematically, it is much more convenient to handle Green-Matsubara's functions $\tilde{G}_{mn}(\tau)$ (also known as imaginary-time Green's functions), defined as:

$$\tilde{G}_{nm}(\tau) = -\hbar\,\mathrm{tr}\left(\hat{\rho}^{(0)} T c_n(\tau) c_m^\dagger(0)\right), \quad \text{with} \quad c_i(\tau) = e^{\tau\mathcal{H}_0}\, c_i\, e^{-\tau\mathcal{H}_0}, \tag{2}$$

and where T is the time ordering operator. Theses functions admit a Fourier series expansion:

$$\tilde{G}_{nm}(\tau) = \frac{1}{b}\sum_{\nu=-\infty}^{+\infty} e^{-\imath\hbar\omega_\nu\tau}\,\tilde{G}_{nm}(\imath\omega_v) \quad \text{with} \quad \tilde{G}_{nm}(\imath\omega_v) = \int_0^b \mathrm{d}\tau\,\tilde{G}_{nm}(\tau)\, e^{\imath\hbar\omega_\nu\tau}. \tag{3}$$

If $|n\rangle$ and $|m\rangle$ depict fermion states, the Matsubara frequencies read:

$$\hbar\omega_\nu = \frac{\pi}{b}(2\nu+1), \quad \nu \in \mathbb{Z}, \tag{4}$$

while they read:

$$\hbar\omega_\nu = \frac{\pi}{b}2\nu, \quad \nu \in \mathbb{Z}, \tag{5}$$

if $|n\rangle$ and $|m\rangle$ depict boson states. Actually, the Matsubara frequencies are respectively defined as the poles of the Fermi-Dirac distribution ρ_+ (for fermions) and the Bose-Einstein distribution ρ_- (for bosons):

$$\rho_\pm(z) = \frac{1}{e^{\hbar b z} \pm 1}, \quad z \in \mathbb{C}. \tag{6}$$

Because retarded Green's functions and Green-Matsubara functions both derive from the Hilbert transform of the same function (the spectral function), they satisfy a simple relationship thanks to analytical continuity of the Hilbert transform over the $\mathbb{C}$-plane: when we replace the Matsubara frequency $\imath\omega_\nu \in \imath\mathbb{R}$ by $(\omega + \imath\gamma) \in \mathbb{C}$ within $\tilde{G}_{nm}(\imath\omega_\nu)$, we retrieve the Fourier transform $G_{nm}(\omega)$ of the retarded Green function $G_{nm}(t)$, for $\gamma \to 0^+$. In other words:

$$G_{mn}(\omega) = \tilde{G}_{mn}(\omega + \imath 0^+). \tag{7}$$

The same principle (enforced in Feynman rule #11) is applied within our method to calculate the optical response functions, which are retarded Green's functions of photon states in real frequency domain. For instance, for second-order hyperpolarizabilities, we have:

$$\beta(\omega_1, \omega_2) = \tilde{\beta}(\omega_1 + \imath 0^+, \omega_2 + \imath 0^+), \tag{8}$$

where the Green-Matsubara's function $\tilde{\beta}$ is defined with respect to the boson Matsubara frequencies $(\imath\omega_\eta, \imath\omega_\kappa)$ defined as the poles of the Bose-Einstein functions describing the distribution of the photon frequencies ω_1 and ω_2 within the input optical beams.

2.2 Rule #8: Signature of optical loop diagrams

In solid-state physics, the derivation of the Feynman rules lies on the application of the Wick theorem which implies a multiplication by the signature $(-1)^{n+L}$, where n is the perturbative order of the diagram (i.e. the number of virtual bosons) and L the number of loops (related to the same N-particle system).

In optics, the dielectric response of a system to an excitation electric field $\mathbf{E}(\omega)$ is characterized by its dipole moment $\mathbf{p}(\omega)$. Optical response functions (also called susceptibilities in the frequency domain)

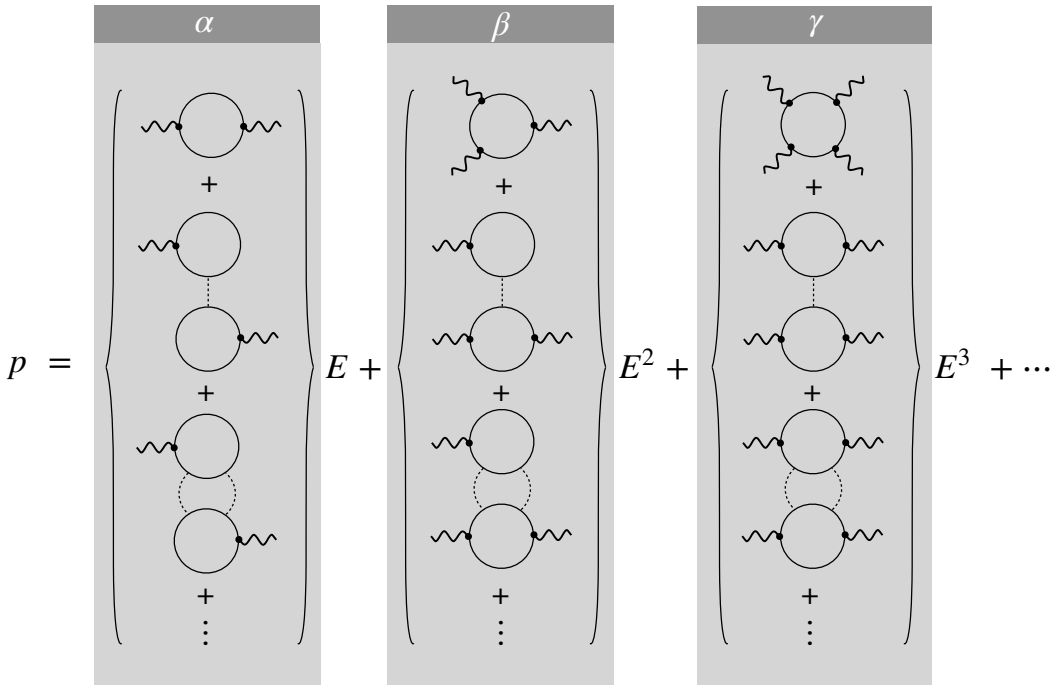

Figure S2: **Perturbative expansion.** In optics, there is no ordering between diagrams according to their number of virtual/vector bosons (dashed lines), but with respect to their number of input/output photons (waved lines). All the diagrams of a same column are made of the same number N_p of photons.

are then defined through the perturbation expansion of $\mathbf{p}(\omega)$ with respect to $\mathbf{E}(\omega)$:

$$
\begin{aligned}
p_i(\omega) \;=\; & \alpha_{ij}(\omega)\, E_j(\omega) && (9)\\
& + \int \mathrm{d}\omega'\; \beta_{ijk}(\omega', \omega-\omega')\, E_j(\omega')\, E_k(\omega-\omega') && (10)\\
& + \iint \mathrm{d}\omega'\, \mathrm{d}\omega''\; \gamma_{ijkl}(\omega', \omega'', \omega-\omega'-\omega'')\, E_j(\omega')\, E_k(\omega'')\, E_l(\omega-\omega'-\omega'') && (11)\\
& + \cdots
\end{aligned}
$$

In terms of diagrams, this expansion can be seen as a sum of contributions of $N_p = 2$ photons (α), $N_p = 3$ photons (β), $N_p = 4$ photons (γ), etc. (see Figure S2). Therefore, $n = N_p$ plays the role of n in the signature. Here, it corresponds to the number of input/output photons which drive the order of the perturbative expansion with respect to the electric field. Moreover, in the case of composite systems, each subsystem is only described by one loop. By construction, $L = 1$: the quantum states of each sub-unit propagate only once (there is a unique fermion Matsubara frequency per sub-unit). As a result, the signature of optical loop diagrams is given by $(-1)^{N_p+1}$, as stated by rule #8.

2.3 Rule #8: Counting of internal Matsubara frequencies

In the theory of Feynman diagrams, we count one factor $1/b$ for each sum over a Matsubara frequency. In practice, if N_f internal Matsubara frequencies intervene within a loop diagram, the computation of the associated Green's function includes a factor b^{-N_f}. In Ref. [1], we count as many internal Matsubara frequencies as subsystems N_l, so that we would have $N_f = N_l$. However, there are hidden Matsubara frequencies that lead to $N_f = N_v - N_p + 1$.

Let us consider the example of the diagram $[2, 1, \downarrow\uparrow]$ (Figure 2), for which $N_l = 2$. As there are two virtual bosons, the conservation of energy at vertices allows the propagation of a boson Matsubara frequency $\hbar\omega_\alpha = \frac{\pi}{b}\, 2\alpha$, $\alpha \in \mathbb{Z}$, as represented in Figure S1. Hence, $N_f = 3 \neq N_l = 2$. For a diagram made of three virtual bosons, like $[3, 0, \downarrow\uparrow]$ (Figure 3), we are allowed to propagate two boson Matsubara frequencies, and $N_f = 4 \neq N_l = 2$. The correct way to count the total number of Matsubara frequencies is illustrated by the Figure S3. First, a diagram is always made of one loop at least. In this case, $N_f = 1$. Second, for a system of N_l sub-units, we have $(N_l - 1)$ virtual bosons at least, which is the minimum

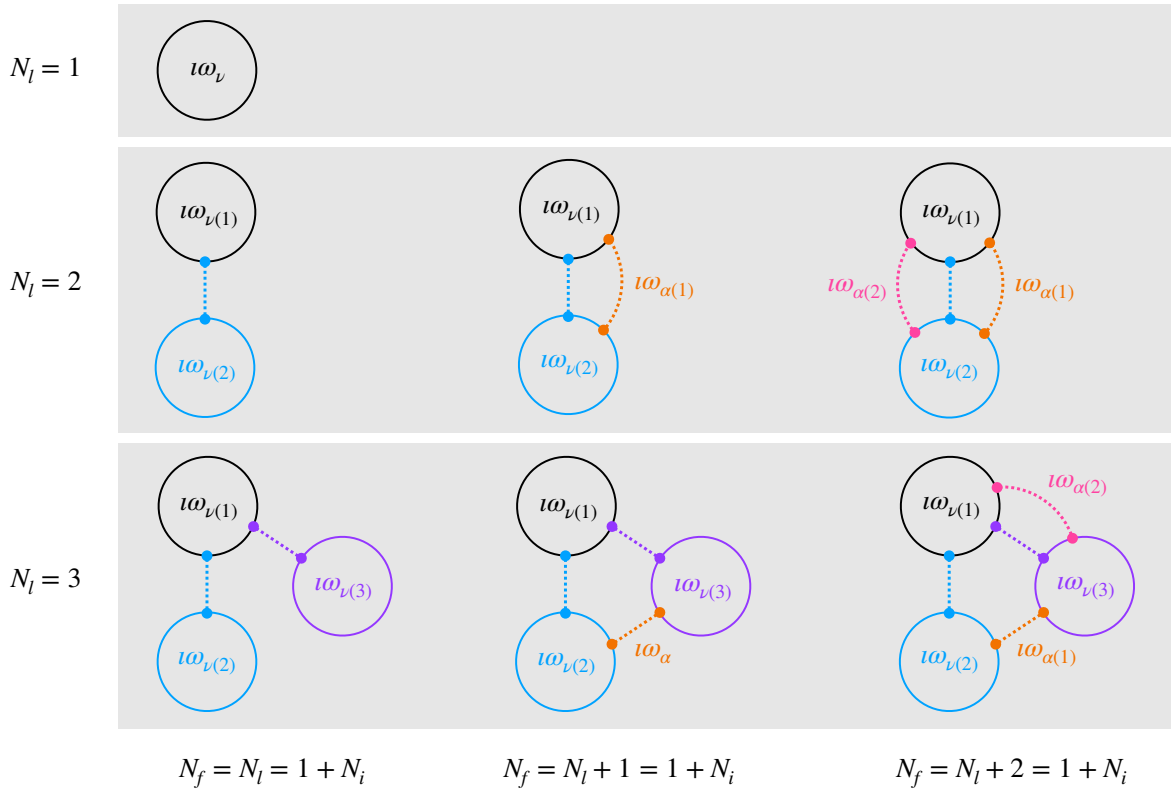

Figure S3: **Internal Matsubara frequencies.** Illustration of the counting of the Matsubara frequencies according to the number of subsystems (N_l loops) and the number of interactions (N_i) between them. The fermion Matsubara frequencies are written with labels ν, while boson Matsubara frequencies are written with labels α. For a given N_l, the minimum number of virtual bosons to connect the subsystem is $N_i = N_l - 1$. In this case, $N_f = N_l$. As soon as $N_i > N_l - 1$, each additional virtual boson introduces a new boson Matsubara frequency: we have N_l fermion frequencies $\imath\omega_\nu$ and $(N_i - N_l + 1)$ boson frequencies. Hence, in all cases, the total number of Matsubara frequencies is given by $N_f = 1 + N_i$.

number of connections to get an interacting composite system. Because of the conservation of energy at vertices, the frequencies of theses $(N_l - 1)$ virtual bosons are fixed, so that they do not introduce new degrees of freedom over the Matsubara frequencies. At this stage, we count $N_f = 1 + N_i$ Matsubara frequencies, where N_i is the number of interactions, here equal to the number $(N_l - 1)$ of additional sub-units (compared to a 1-loop diagram). Third, when $N_i > N_l - 1$, each additional virtual boson leads to the introduction of a new degree of freedom, and then to an additional internal Matsubara frequency. The total number of Matsubara frequencies is eventually given by $N_f = 1 + N_i$ in all cases, where N_i is the total number of interactions between sub-units. From the rule #2: $N_i = N_v - N_p$, i.e. $N_f = 1 + N_v - N_p$. This is why the rule #8 states that the response function is characterized by a factor $b^{N_p - N_v - 1} = b^{-N_f}$.

2.4 Rule #5: Matsubara frequencies of virtual bosons

Even though the previous reasoning gives an explanation to rule #8, rule #5 states that we only sum over the Matsubara frequencies associated to the N_l subsystem loops. To understand why, let us call N_d the number of additional degrees of freedom introduced by excess virtual photons (when $N_i > N_l - 1$). We have $N_d = N_i - (N_l - 1) = N_v - N_p - N_l + 1$. The total number of internal Matsubara frequencies is then $N_f = N_l + N_d$. For any N_l-loop diagrams, it is possible to split the N_l sums over the fermion Matsubara frequencies $\{\omega_{\nu(n)}\}_{n=1}^{n=N_l}$ (propagators in fermion loops) from the N_d sums over the boson Matsubara frequencies $\{\omega_{\alpha(n')}\}_{n'=1}^{n'=N_d}$ (virtual boson interaction vertices) within the computation of the

associated Green-Matsubara's function:

$$\tilde{G}(\imath\omega_{\eta(1)},\cdots,\imath\omega_{\eta(N_p)}) = \prod_{n=1}^{N_l}\left(\frac{1}{b}\sum_{\nu(n)}\right)\prod_{n'=1}^{N_d}\left(\frac{1}{b}\sum_{\alpha(n')}\right) f(\imath\omega_{\nu(n)},\imath\omega_{\alpha(n')}), \tag{12}$$

where function f is a product of elementary Green's functions and coupling constants (see in Figure S3 examples of diagrams illustrating the definitions of $\imath\omega_{\nu(n)}$ and $\imath\omega_{\alpha(n')}$). In solid-state physics, the aim is to treat N-body interactions as perturbations and then to sum over all the frequencies which can be propagated within the system through virtual bosons. In this manner, there is an ordering between the processes according to the number of virtual bosons: processes encoded by $(V+1)$ virtual bosons are negligible in comparison with those encoded by V virtual bosons. As discussed previously, the interactions are not treated as perturbations in optical diagrams so that we should talk about vector bosons instead of virtual bosons. This point has an important consequence: as mediators of dipole-dipole interactions, the vector bosons only propagate linear combinations of the optical frequencies $\imath\omega_1,\cdots,\imath\omega_{N_p}$. Let us consider again the diagram $[2,1,\downarrow\uparrow]$ which leads to the computation of $\tilde{\beta}(\imath\omega_\eta,\imath\omega_\kappa)$ (Figure S1). The two vector bosons propagate the Matsubara frequencies $(\imath\omega_\eta+\imath\omega_\alpha)$ and $(\imath\omega_\eta+\imath\omega_\kappa+\imath\omega_\alpha)$. The frequency $\imath\omega_\alpha$ is internal to the system and summed for $\alpha\in\mathbb{Z}$, while $(\imath\omega_\eta,\imath\omega_\kappa)$ are fixed and associated to the input photons (ω_1,ω_2). So, the vector bosons embody real processes if, and only if, $\imath\omega_\eta=\imath\omega_1$, $\imath\omega_\kappa=\imath\omega_2$ and $\imath\omega_\alpha=0$. In the general case of N_p photons of real frequencies $\{\omega_N\}_{N=1}^{N=N_p}$ interacting with a composite system, we are actually interested in the response function:

$$\tilde{G}(\imath\omega_1,\cdots,\imath\omega_{N_p}) = \prod_{N=1}^{N_p}\int_{\mathbb{R}} \mathrm{d}\omega_{\eta(N)}\ \delta(\omega_N-\omega_{\eta(N)})\ \tilde{G}(\imath\omega_{\eta(1)},\cdots,\imath\omega_{\eta(N_p)}). \tag{13}$$

The condition $\omega_{\eta(N)}=\omega_N$ means that it must formally exists an integer $\eta(N)$ so that:

$$\hbar\omega_N = \frac{\pi}{b}2\eta(N). \tag{14}$$

As the optical frequencies ω_N are continuously distributed over $\mathbb{R}$, the real optical response function is deduced from the Green-Matsubara's function $\tilde{G}(\imath\omega_1,\cdots,\imath\omega_{N_p})$ after taking the limit $b\to\infty$, i.e. $T\to 0$. Indeed, $1/b$ quantifies the distance between two consecutive Matsubara frequencies, so that b must tend to the infinity for $\{\omega_{\eta(N)}\}_{\eta(N)\in\mathbb{N}}$ to be dense in $\mathbb{R}$. Moreover, as we do not treat the interactions between subsystems as perturbations, the degrees of freedom introduced by the boson Matsubara frequencies $\omega_{\alpha(n')}$ must be eliminated. In other words, the N_d sums over the boson frequencies must be weighted by Kronecker symbols of type $\delta_{\alpha,0}$:

$$\begin{aligned}
\tilde{G}(\imath\omega_1,\cdots,\imath\omega_{N_p}) &= \prod_{n=1}^{N_l}\left(\frac{1}{b}\sum_{\nu(n)}\right)\prod_{n'=1}^{N_d}\left(\frac{1}{b}\sum_{\alpha(n')}\delta_{\alpha(n'),0}\right) f(\imath\omega_{\nu(n)},\imath\omega_{\alpha(n')}) &(15)\\
&= \frac{1}{b^{N_l}}\prod_{n=1}^{N_l}\sum_{\nu(n)}\frac{1}{b^{N_d}} f(\imath\omega_{\nu(n)},0) &(16)\\
&= (b^{N_p-N_v-1})\prod_{n=1}^{N_l}\sum_{\nu(n)} f(\imath\omega_{\nu(n)},0). &(17)
\end{aligned}$$

For all these reasons, the diagrams are drawn and filled with $(\imath\omega_1,\imath\omega_2)$ instead of $(\imath\omega_\eta,\imath\omega_\kappa)$, and virtual/vector bosons are not associated to internal Matsubara frequencies.

2.5 Rule #9: Summations over quantum states and Matsubara frequencies

Equation (17) shows the general shape of the response function derived from any optical diagram. First, the fermion Matsubara frequencies $\imath\omega_{\nu(n)}$, which are internal variables without direct physical meaning, must be eliminated thanks to the residue theorem. Second, function $f(\imath\omega_{\nu(n)})$ is itself a sum over all the quantum numbers labeling the states of the sub-units composing the system. Interestingly, the application of the residue theorem changes the sums over Matsubara frequencies into sums over the poles z_u of Matsubara-Green's functions weighted by the distribution function $\rho(z_u)$ of Fermi-Dirac and/or its derivatives (as we only deal with fermion Matsubara frequencies, we have to handle function

$\rho_+(z)$ defined by Eq. (6), for which we drop subscript '+' in the following). Here, for each sum over a Matsubara frequency, unambiguously associated to a given sub-unit, the poles z_u depend on the eigen-frequencies ω_m of the sub-unit itself (and a linear combination of the input optical frequencies). The mathematical information encoded by Matsubara frequencies thus translates into physical information about the statistical distribution of the quantum states within the system. As a result, summing over the quantum states $|m\rangle$ introduces statistical selection rules driven by $\rho(\omega_m)$, $\rho'(\omega_m)$, $\rho''(\omega_m)$, etc., which depend on the temperature. This is of high importance as our optical formulation considers the optical response functions as the asymptotic values of the Green-Matsubara's functions at zero temperature. Here we detail the mathematical formulation of these selection rules.

Matsubara frequencies and residue theorem. The residue theorem allows the reduction of sums of products of Green-Matsubara's functions by using the fact that the fermion Matsubara frequencies are the poles of the Fermi-Dirac distribution $\rho(z)$. It states that for all meromorphic function ϕ characterized by N simple poles $\{z_u\}_{1\leqslant u\leqslant N}$ and the associated residues $\{r_u\}_{1\leqslant u\leqslant N}$ [1]:

$$\frac{1}{b}\sum_{\nu}\phi(\imath\omega_\nu) = \hbar\sum_{u} r_u\ \rho(z_u). \tag{18}$$

In the general case of multiple poles, we have:

$$\frac{1}{b}\sum_{\nu}\phi(\imath\omega_\nu) = \hbar\sum_{u} \mathrm{Res}_{z_u}[\rho(z)\phi(z)]. \tag{19}$$

Residues are then computed from:

$$\mathrm{Res}_a(f) = \frac{1}{(n-1)!}\lim_{z\to a}\frac{\partial^{n-1}}{\partial z^{n-1}}\left[(z-a)^n f(z)\right], \qquad \text{with} \qquad f(z)=\rho(z)\phi(z). \tag{20}$$

Derivatives of the Fermi-Dirac distribution. It is worth noting that the first derivative of $\rho(z)$ can be expressed with $\rho(z)$ itself:

$$\rho'(z) = \hbar b\,\rho(z)\,(\rho(z)-1). \tag{21}$$

As a consequence, for $z\in\mathbb{R}$, the limit $T\to 0$ ($b\to\infty$) leads to:

	$\rho(z)$	$\rho(z)-1$	$\rho'(z)$
$z>0$	$\sim e^{-\hbar b z}$	~ -1	$\sim -\hbar b\, e^{-\hbar b z}$
$z<0$	~ 1	$\sim -e^{\hbar b z}$	$\sim -\hbar b\, e^{\hbar b z}$

Then, in the zero temperature limit:

$$\frac{\sup_{z\in\mathbb{R}}|\rho'(z)|}{\sup_{z\in\mathbb{R}}|\rho(z)|}\sim\hbar b \qquad\Longrightarrow\qquad \sup_{z\in\mathbb{R}}|\rho'(z)| \gg \sup_{z\in\mathbb{R}}|\rho(z)|. \tag{22}$$

In other words, when a quantity sums up on states $|m\rangle$ different contributions respectively weighted by $\rho'(\omega_m)$ and $\rho(\omega_m)$, the low temperature limit comes down to selecting the sole terms weighted by $\rho'(\omega_m)$, as they are dominant inside the sum. Typically, for all functions f and g satisfying $f \underset{T\to 0}{\sim} g$:

$$\sum_m \big(\rho'(\omega_m)\,f(\omega_m)+\rho(\omega_m)\,g(\omega_m)\big) \underset{T\to 0}{\longrightarrow} \sum_m \rho'(\omega_m)\,f(\omega_m), \tag{23}$$

and the sum reduced to the terms weighted by $\rho'(\omega_m)$ contains all the significant contributions when $T\to 0$. This result can be generalized for all the successive derivatives $\rho^{(n)}(z)$ of $\rho(z)$, as their leading terms are:

$$\rho^{(n)}(z) = \frac{\mathrm{d}^n\rho}{\mathrm{d}z^n} = (\hbar b)^n\rho(z)\left[n!\,\rho^n(z)+\cdots\right]. \tag{24}$$

Hence, for all $n>n'$:

$$\frac{\sup_{z\in\mathbb{R}}|\rho^{(n)}(z)|}{\sup_{z\in\mathbb{R}}|\rho^{(n')}(z)|}\sim(\hbar b)^{n-n'} \qquad\Longrightarrow\qquad \sup_{z\in\mathbb{R}}|\rho^{(n)}(z)| \gg \sup_{z\in\mathbb{R}}|\rho^{(n')}(z)|. \tag{25}$$

Taking the low temperature limit within a sum over quantum states thus leads to only keeping the contributions weighted by the highest order derivative. Combined with the residue theorem (eq. (19)) and the derivative character of the calculation of the residues (eq. (20)), this condition of higher derivative order translates into a condition of higher multiplicity of the poles. When performing the sum of a meromorphic function ϕ over Matsubara frequencies as in equation (19), selecting the contributions of higher derivative order $\rho^{(n)}$ conveys into selecting only the contributions of the $(n+1)$-multiple poles of function ϕ.

3 Canonical linear and nonlinear optical response functions

3.1 First-order polarizability

As previously derived from the Feynman rules governing the loop diagram formalism [1], the 1st-order response function $\alpha_{ij}(\omega)$ of a simple system is given by the loop diagram of Figure S4(a). In imaginary frequency (Matsubara formalism), it reads:

$$\alpha_{ij}(\imath\omega) = \frac{-1}{b\hbar^2} \sum_{m,n} \sum_{\nu} p^i_{mn}\, p^j_{nm}\, \tilde{G}_m(\imath\omega_\nu)\, \tilde{G}_n(\imath\omega_\nu + \imath\omega). \tag{26}$$

where $\mathbf{p}$ is the dipole moment, $b = 1/(k_B T)$, and:

$$\tilde{G}_m(z) = \frac{1}{z - \omega_m}. \tag{27}$$

This actually corresponds to the smallest unit diagram of optics. The calculation leads to [1]:

$$\alpha_{ij}(\imath\omega) = \frac{1}{\hbar} \sum_{m} \hat{\rho}_{mm} \sum_{n} \left(\frac{p^i_{mn} p^j_{nm}}{\omega_{nm} - \imath\omega} + \frac{p^j_{mn} p^i_{nm}}{\omega_{nm} + \imath\omega} \right), \tag{28}$$

which gives, after application of rules #11 and 12:

$$\alpha_{ij}(\omega) = \frac{-1}{\hbar} \sum_{m,n} \hat{\rho}_{mm} \left(\frac{p^i_{mn} p^j_{nm}}{\omega - \omega_{nm} + \imath\Gamma_{nm}} - \frac{p^j_{mn} p^i_{nm}}{\omega + \omega_{nm} + \imath\Gamma_{nm}} \right). \tag{29}$$

In imaginary frequencies, the polarizability conveniently separates into:

$$\alpha_{ij}(\imath\omega) = \alpha^-_{ij}(\imath\omega) + \alpha^+_{ji}(\imath\omega), \qquad \text{with} \qquad \alpha^\pm_{ij}(\imath\omega) = \frac{\pm 1}{\hbar} \sum_{m} \hat{\rho}_{mm} \sum_{n} \frac{p^i_{mn} p^j_{nm}}{\imath\omega \pm \omega_{nm}}. \tag{30}$$

These two terms α^-_{ij} and α^+_{ji} can be seen as the resonant and non-resonant parts of the linear polarizability α_{ij}, respectively. It is worth noting that $\alpha^-_{ij}(\imath\omega) = \alpha^+_{ij}(-\imath\omega)$.

3.2 Second-order hyperpolarizability

In the case of 2nd-order processes like SFG, we must consider two 1-loop diagrams (Figure S4(b)), as deduced from the Feynman rules. The first diagram, associated to the cyclic permutation (1 2 3), leads to:

$$\beta^{(123)}_{ijk}(\imath\omega_1, \imath\omega_2) = \frac{1}{b\hbar^3} \sum_{m,n,q} \sum_{\nu} p^i_{mq}\, p^j_{nm}\, p^k_{qn}\, \tilde{G}_m(\imath\omega_\nu)\, \tilde{G}_n(\imath\omega_\nu + \imath\omega_1)\, \tilde{G}_q(\imath\omega_\nu + \imath\omega_3), \tag{31}$$

with $\omega_3 = \omega_1 + \omega_2$. The second one, associated to the permutation (2 1 3), can be expressed as:

$$\beta^{(213)}_{ijk}(\imath\omega_1, \imath\omega_2) = \beta^{(123)}_{ikj}(\imath\omega_2, \imath\omega_1). \tag{32}$$

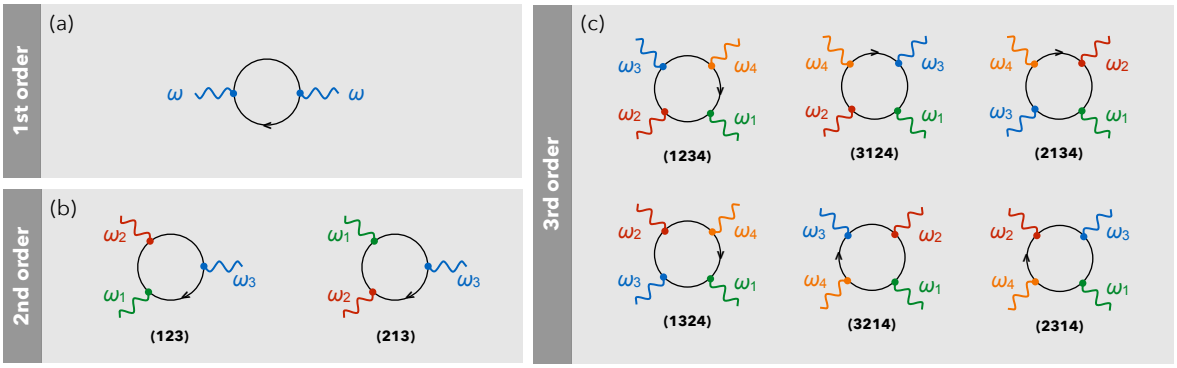

Figure S4: **Simple systems.** Complete list of Feynman diagrams accounting for first-, second-, and third-order optical responses of one-body systems. Diagrams are labeled by the associated cyclic permutations.

The total 2nd-order response function of a simple system consists in the sum of these two contribution: $\beta_{ijk}(\imath\omega_1,\imath\omega_2) = \beta^{(123)}_{ijk}(\imath\omega_1,\imath\omega_2) + \beta^{(213)}_{ijk}(\imath\omega_1,\imath\omega_2)$, as shown in Ref. 1. After application of rules #10 to 12, we get [1]:

$$\begin{aligned}\beta_{ijk}(\omega_1,\omega_2) = & \qquad (33)\\ \frac{1}{\hbar^2}\sum_{m,n,l}\hat{\rho}_{ll} \Bigg[& \frac{p^i_{ln}p^j_{ml}p^k_{nm}}{(\omega_{nl}-\omega_3-\imath\Gamma_{nl})(\omega_{ml}-\omega_1-\imath\Gamma_{ml})} + \frac{p^i_{nm}p^j_{ln}p^k_{ml}}{(\omega_{nm}+\omega_3+\imath\Gamma_{nm})(\omega_{ml}-\omega_2-\imath\Gamma_{ml})}\\ + & \frac{p^i_{nm}p^j_{ln}p^k_{ml}}{(\omega_{mn}-\omega_3-\imath\Gamma_{mn})(\omega_{nl}+\omega_1+\imath\Gamma_{nl})} + \frac{p^i_{ml}p^j_{nm}p^k_{ln}}{(\omega_{ml}+\omega_3+\imath\Gamma_{ml})(\omega_{nl}+\omega_2+\imath\Gamma_{nl})}\\ + & \frac{p^i_{ln}p^j_{nm}p^k_{ml}}{(\omega_{nl}-\omega_3-\imath\Gamma_{nl})(\omega_{ml}-\omega_2-\imath\Gamma_{ml})} + \frac{p^i_{nm}p^j_{ml}p^k_{ln}}{(\omega_{nm}+\omega_3+\imath\Gamma_{nm})(\omega_{ml}-\omega_1-\imath\Gamma_{ml})}\\ + & \frac{p^i_{nm}p^j_{ml}p^k_{ln}}{(\omega_{mn}-\omega_3-\imath\Gamma_{mn})(\omega_{nl}+\omega_2+\imath\Gamma_{nl})} + \frac{p^i_{ml}p^j_{ln}p^k_{nm}}{(\omega_{ml}+\omega_3+\imath\Gamma_{ml})(\omega_{nl}+\omega_1+\imath\Gamma_{nl})} \Bigg].\end{aligned}$$

3.3 Third-order hyperpolarizability

Since 3rd-order processes imply four photons (i.e. three input frequencies), we count as many diagrams as cyclic permutations of order 4, that is 3! = 6 (Figure S4(c)). Here we give the response function corresponding to the diagram (1 2 3 4), as derived from the application of the Feynman rules:

$$\begin{aligned}&\gamma^{(1234)}_{ijkl}(\imath\omega_1,\imath\omega_2,\imath\omega_3) =\\ &\quad\frac{-1}{b\hbar^4}\sum_{m,n,q,r}\sum_{\nu} p^i_{mr}\,p^j_{nm}\,p^k_{qn}\,p^l_{rq}\,\tilde{G}_m(\imath\omega_\nu)\,\tilde{G}_n(\imath\omega_\nu+\imath\omega_1)\,\tilde{G}_q(\imath\omega_\nu+\imath\omega_1+\imath\omega_2)\,\tilde{G}_r(\imath\omega_\nu+\imath\omega_4), \qquad (34)\end{aligned}$$

with $\omega_4 = \omega_1+\omega_2+\omega_3$. The complete 3rd-order response function is then the sum of the 6 diagrams:

$$\gamma_{ijkl}(\imath\omega_1,\imath\omega_2,\imath\omega_3) = \sum_{\sigma\in\mathfrak{S}_4}\gamma^{(\sigma)}_{ijkl}(\imath\omega_1,\imath\omega_2,\imath\omega_3), \qquad (35)$$

where $\mathfrak{S}_4$ depicts the set of the cyclic permutations of order 4. Each $\gamma^{(\sigma)}_{ijkl}$ can be deduced from (34):

$$\gamma^{(2314)}_{ijkl}(\imath\omega_1,\imath\omega_2,\imath\omega_3) = \gamma^{(1234)}_{iklj}(\imath\omega_2,\imath\omega_3,\imath\omega_1),\quad \gamma^{(1324)}_{ijkl}(\imath\omega_1,\imath\omega_2,\imath\omega_3) = \gamma^{(1234)}_{ijlk}(\imath\omega_1,\imath\omega_3,\imath\omega_2),\quad \text{etc.} \qquad (36)$$

3.4 Fifth-order hyperpolarizability

Even though optical processes of 5th-order are not studied experimentally, our derivation of the response functions associated to 3-boson diagrams (Figure 3) involves the 5th-order response function of the substrate. This is well defined on a mathematical point view by:

$$\begin{aligned}&\xi^{(123456)}_{ijkluv}(\imath\omega_1,\imath\omega_2,\imath\omega_3,\imath\omega_4,\imath\omega_5) = \frac{-1}{b\hbar^6}\sum_{m,n,q,r,s,t}\sum_{\nu} p^i_{mt}\,p^j_{nm}\,p^k_{qn}\,p^l_{rq}\,p^u_{sr}\,p^v_{ts}\\ &\tilde{G}_m(\imath\omega_\nu)\,\tilde{G}_n(\imath\omega_\nu+\imath\omega_1)\,\tilde{G}_q(\imath\omega_\nu+\imath\omega_{1,2})\tilde{G}_r(\imath\omega_\nu+\imath\omega_{1,2,3})\,\tilde{G}_s(\imath\omega_\nu+\imath\omega_{1,2,3,4})\,\tilde{G}_t(\imath\omega_\nu+\imath\omega_{1,2,3,4,5}), \qquad (37)\end{aligned}$$

where we concisely write $\omega_{1,\cdots,n} = \omega_1+\cdots+\omega_n$. This functions is represented in Figure S5.

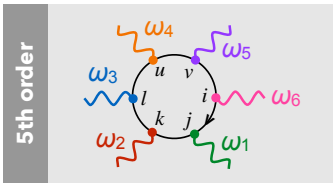

Figure S5: Diagrammatic representation of $\xi^{(123456)}_{ijkluv}(\imath\omega_1,\imath\omega_2,\imath\omega_3,\imath\omega_4,\imath\omega_5)$, with $\omega_6 = \sum_{n=1}^{5}\omega_n$.

4 Factorization of odd-order response functions

In Figures 2 and 3, we show that the diagrams made of 2 and 3 virtual bosons lead to 2nd-order response functions of the system which can be factorized by 3rd- and 5th-order response functions of the nanoparticle. Indeed, the upper loops of these diagrams are respectively made of 4 and 6 propagators. Interestingly, these 3rd- and 5th-order response functions can be split into products of simple 1st-order response functions. In this section, we demonstrate this mathematical property for any odd-order response function.

4.1 Factorization of third-order functions γ_{ijkl}

The third-order response functions γ_{ijkl} are sometimes split into the product of two first-order functions $\alpha_{ij}\,\alpha_{kl}$, i.e. "$\gamma_{ijkl} \propto \alpha_{ij}\,\alpha_{kl}$" or "$\boldsymbol{\gamma} \propto \boldsymbol{\alpha} \otimes \boldsymbol{\alpha}$". But here are two significant inaccuracies of this splitting: first, the two pairs of components (i,j) and (k,l) are coupled through γ_{ijkl}, while they are not anymore within $\alpha_{ij}\,\alpha_{kl}$; second, γ_{ijkl} is a function of three frequencies, while $\alpha_{ij}\,\alpha_{kl}$ is a function of two frequencies (at most).

Actually, it is solely possible to factorize third-order functions in very specific cases: they must explicitly depend on two frequencies only and, as we will see below, they must arise from a composite diagram containing hidden boson Matsubara frequencies, i.e. satisfying $N_v - N_p > N_l - 1$ (Part 2.4). Under these conditions:

$$\frac{1}{b}\,\gamma_{ijkl}^{(1234)}(\imath\omega, -\imath\omega, \imath\omega') = -\,\alpha_{il}^{-}(\imath\omega')\,\alpha_{kj}^{-}(\imath\omega), \tag{38}$$

where $\alpha_{uv}^{-}(\omega)$ is the resonant part of $\alpha_{uv}(\omega)$, defined in Eq. (30), and $1/b = k_B T$ is the thermal energy. This result is illustrated by loop diagrams in Figure S6. We notice that the relation in Eq. (38) is homogeneous, as $[pE] = [\alpha E^2] = [\gamma E^4]$ (where p is a dipole moment and E an electric field) is an energy, like $[1/b]$. This implies that $[\alpha] = [\gamma E^2]$ and, therefore, $[1/b \cdot \gamma] = [\gamma \alpha E^2] = [\alpha]^2$.

To demonstrate equation (38), we first write, in imaginary frequencies:

$$\frac{1}{b}\,\gamma_{ijkl}^{(1234)}(\imath\omega, -\imath\omega, \imath\omega') = \frac{-1}{b^2\hbar^4}\sum_{\nu}\sum_{mnqr} p_{mr}^{i} p_{nm}^{j} p_{qn}^{k} p_{rq}^{l}\,\tilde{G}_m(\imath\omega_\nu)\tilde{G}_n(\imath\omega_\nu + \imath\omega)\tilde{G}_q(\imath\omega_\nu)\tilde{G}_r(\imath\omega_\nu + \imath\omega'), \tag{39}$$

and:

$$\begin{aligned}
\alpha_{kj}(\imath\omega)\,\alpha_{il}(\imath\omega') &= \frac{1}{b^2\hbar^4}\sum_{m,n}\sum_{\nu} p_{mn}^{k}\,p_{nm}^{j}\,\tilde{G}_m(\imath\omega_\nu)\,\tilde{G}_n(\imath\omega_\nu + \imath\omega)\sum_{q,r}\sum_{\lambda} p_{qr}^{i}\,p_{rq}^{l}\,\tilde{G}_q(\imath\omega_\lambda)\,\tilde{G}_r(\imath\omega_\lambda + \imath\omega') \\
&= \frac{1}{b^2\hbar^4}\sum_{\nu,\lambda}\sum_{mnqr} p_{qr}^{i}\,p_{nm}^{j}\,p_{mn}^{k}\,p_{rq}^{l}\,\tilde{G}_m(\imath\omega_\nu)\,\tilde{G}_n(\imath\omega_\nu + \imath\omega)\,\tilde{G}_q(\imath\omega_\lambda)\,\tilde{G}_r(\imath\omega_\lambda + \imath\omega'). \qquad (40)
\end{aligned}$$

We notice that the two expressions coincide when $m = q$ in (39), and $(m,\nu) = (q,\lambda)$ in (40). In order to formally account for this, we define the linear operators $\{\cdot\}^{*/\dagger}$ extracting the contributions for which $m = q$ and $\nu = \lambda$, respectively:

$$\left\{\sum_{mnqr} f_{mnqr}\right\}^{*} = \sum_{mnqr} f_{mnqr}\,\delta_{mq} = \sum_{mnr} f_{mnmr}, \tag{41}$$

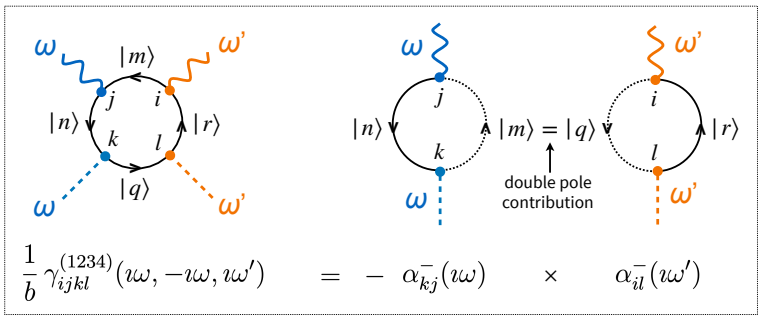

Figure S6: **Factorization of γ functions.** Diagrammatic representation of equation (38).

and:

$$\left\{\sum_{\nu\lambda} f(\imath\omega_\nu,\imath\omega_\lambda)\right\}^\dagger = \sum_{\nu\lambda} f(\imath\omega_\nu,\imath\omega_\lambda)\,\delta_{\nu\lambda} = \sum_{\nu} f(\imath\omega_\nu,\imath\omega_\nu). \tag{42}$$

Henceforth:

$$\left\{\frac{1}{b}\,\gamma^{(1234)}_{ijkl}(\imath\omega,-\imath\omega,\imath\omega')\right\}^* = -\left\{\{\alpha_{kj}(\imath\omega)\,\alpha_{il}(\imath\omega')\}^\dagger\right\}^*. \tag{43}$$

Let us focus first on the product $\alpha_{kj}\,\alpha_{il}$. It derives from the function:

$$f_{mnqr}(\imath\omega_\nu,\imath\omega_\lambda) = p^i_{qr}\,p^j_{nm}\,p^k_{mn}\,p^l_{rq}\;\phi_{mn}(\imath\omega_\nu,\imath\omega)\,\psi_{qr}(\imath\omega_\lambda,\imath\omega') \tag{44}$$

with:

$$\phi_{mn}(\imath\omega_\nu,\imath\omega) = \tilde{G}_m(\imath\omega_\nu)\,\tilde{G}_n(\imath\omega_\nu+\imath\omega) \quad \text{and} \quad \psi_{qr}(\imath\omega_\lambda,\imath\omega') = \tilde{G}_q(\imath\omega_\lambda)\,\tilde{G}_r(\imath\omega_\lambda+\imath\omega'). \tag{45}$$

After applying operator $\{\cdot\}^\dagger$, the double sum over the Matsubara frequencies in Eq. (40) reduces to:

$$\left\{\frac{1}{b^2}\sum_{\nu,\lambda}\phi_{mn}(\imath\omega_\nu,\imath\omega)\,\psi_{qr}(\imath\omega_\lambda,\imath\omega')\right\}^\dagger = \frac{1}{b^2}\sum_{\nu}\underbrace{\phi_{mn}(\imath\omega_\nu,\imath\omega)\,\psi_{qr}(\imath\omega_\nu,\imath\omega')}_{=\Phi_{mnqr}(\imath\omega_\nu,\imath\omega,\imath\omega')}. \tag{46}$$

The application of the residue theorem depends on the multiplicity of the poles (see Part 2.5). For all $(\omega,\omega')\in\mathbb{R}^2$, the function Φ only gets simple poles except if $m=q$. In this case, $\omega_m=\omega_q$ is indeed a double pole of $z\mapsto\Phi_{mnmr}(z,\imath\omega,\imath\omega')$:

$$\Phi_{mnmr}(\imath\omega_\nu,\imath\omega,\imath\omega') = \frac{1}{(\imath\omega_\nu-\omega_m)^2}\,\frac{1}{\imath\omega_\nu+\imath\omega-\omega_n}\,\frac{1}{\imath\omega_\nu+\imath\omega'-\omega_r}. \tag{47}$$

The associated residue is (eq. (19)):

$$\mathrm{Res}_{\omega_m}(\rho\Phi) = \frac{\rho'(\omega_m)}{(\omega_{mn}+\imath\omega)(\omega_{mr}+\imath\omega')} - \rho(\omega_m)\cdot\frac{\omega_{mn}+\omega_{mr}+\imath(\omega+\omega')}{(\omega_{mn}+\imath\omega)^2(\omega_{mr}+\imath\omega')^2}, \tag{48}$$

while the residues associated to the two other simple poles $(\omega_n-\imath\omega)$ and $(\omega_r-\imath\omega')$ are:

$$\mathrm{Res}_{\omega_n-\imath\omega}(\rho\Phi) = \frac{\rho(\omega_n)}{(\omega_{nm}-\imath\omega)^2(\omega_{nr}+\imath\omega'-\imath\omega)},\ \mathrm{Res}_{\omega_r-\imath\omega'}(\rho\Phi) = \frac{\rho(\omega_r)}{(\omega_{rm}-\imath\omega')^2(\omega_{rn}+\imath\omega-\imath\omega')}. \tag{49}$$

When $m\neq q$, all the poles are simple and the associated residues have the same form than those of Eq. (49), i.e. weighted by $\rho(\omega_i)$. As discussed in Part 2.5, the dominant contribution when $T\to 0$ (i.e. $b\to\infty$) is then driven by the derivative $\rho'(\omega_m)$ arising from the double poles when $m=q$. This means that selecting the cases $m=q$ comes down to taking the limit $T\to 0$:

$$\left\{\{\alpha_{kj}(\imath\omega)\,\alpha_{il}(\imath\omega')\}^\dagger\right\}^* = \lim_{T\to 0}\{\alpha_{kj}(\imath\omega)\,\alpha_{il}(\imath\omega')\}^\dagger. \tag{50}$$

This result is also valid for $\gamma^{(1234)}$, which derives from:

$$f_{mnqr}(\imath\omega_\nu,\imath\omega_\lambda) = p^i_{mr}\,p^j_{nm}\,p^k_{qn}\,p^l_{rq}\;\phi_{mn}(\imath\omega_\nu,\imath\omega)\,\psi_{qr}(\imath\omega_\nu,\imath\omega'), \tag{51}$$

with the difference that we directly get $\Phi_{mnqr}(\imath\omega_\nu,\imath\omega,\imath\omega')$ since there is a unique sum over ν, i.e. no contribution over λ, unlike Eq. (46). The dominant contribution at zero temperature is again deduced from the double pole $m=q$:

$$\left\{\frac{1}{b}\,\gamma^{(1234)}_{ijkl}(\imath\omega,-\imath\omega,\imath\omega')\right\}^* = \lim_{T\to 0}\frac{1}{b}\,\gamma^{(1234)}_{ijkl}(\imath\omega,-\imath\omega,\imath\omega'). \tag{52}$$

This contribution reads:

$$\left\{\frac{1}{b}\,\gamma^{(1234)}_{ijkl}(\imath\omega,-\imath\omega,\imath\omega')\right\}^* = \frac{-1}{b\hbar^3}\sum_{mnr} p^k_{mn}p^j_{nm}p^i_{mr}p^l_{rm}\,\frac{\rho'(\omega_m)}{(\omega_{mn}+\imath\omega)(\omega_{mr}+\imath\omega')}, \tag{53}$$

that is, following equation (43):

$$\Big\{\{\alpha_{kj}(\imath\omega)\,\alpha_{il}(\imath\omega')\}^{\dagger}\Big\}^{*} = \frac{-1}{b\hbar^3}\sum_m \rho'(\omega_m)\sum_n \frac{p^k_{mn}p^j_{nm}}{\imath\omega-\omega_{nm}}\sum_r \frac{p^i_{mr}p^l_{rm}}{\imath\omega'-\omega_{rm}}. \tag{54}$$

This expression evidences a double resonance $\imath\omega = \omega_{nm}$ and $\imath\omega' = \omega_{rm}$, which means that it derives from the product of two resonant α^- functions (Eq. (30)). Actually, we know that the observable polarizability product splits into:

$$\alpha_{kj}(\imath\omega)\,\alpha_{il}(\imath\omega') = \alpha^-_{kj}(\imath\omega)\,\alpha^-_{il}(\imath\omega') + \alpha^+_{jk}(\imath\omega)\,\alpha^-_{il}(\imath\omega') + \alpha^-_{kj}(\imath\omega)\,\alpha^+_{li}(\imath\omega') + \alpha^+_{jk}(\imath\omega)\,\alpha^+_{li}(\imath\omega'). \tag{55}$$

Among these four terms, only the first one fulfills the same double resonance condition as in Eq. (54). To satisfy (50), we then have:

$$\lim_{T\to 0}\{\alpha_{kj}(\imath\omega)\,\alpha_{il}(\imath\omega')\}^{\dagger} = \lim_{T\to 0}\alpha^-_{kj}(\imath\omega)\,\alpha^-_{il}(\imath\omega'). \tag{56}$$

As a conclusion, equation (43) leads to:

$$\lim_{T\to 0}\frac{1}{b}\,\gamma^{(1234)}_{ijkl}(\imath\omega,-\imath\omega,\imath\omega') = -\lim_{T\to 0}\alpha^-_{kj}(\imath\omega)\,\alpha^-_{il}(\imath\omega'). \tag{57}$$

Given that the limit at low temperature is implicitly taken when we apply the Matsubara formalism to the calculation of optical response functions (see Part 1), this equation is identified to (38).

4.2 Factorization of fifth-order functions ξ_{ijkluv}

For 3-boson bipartite diagrams (Figure 3), we deal with the response function:

$$\xi^{(123456)}_{ijkluv}(\imath\omega_1,-\imath\omega_1,\imath\omega_2,-\imath\omega_2,\imath\omega_3) = \frac{-1}{b\hbar^6}\sum_{m,n,q,r,s,t;\nu} p^i_{mt}\,p^j_{nm}\,p^k_{qn}\,p^l_{rq}\,p^u_{sr}\,p^v_{ts}$$
$$\tilde{G}_m(\imath\omega_\nu)\,\tilde{G}_n(\imath\omega_\nu+\imath\omega_1)\,\tilde{G}_q(\imath\omega_\nu)\tilde{G}_r(\imath\omega_\nu+\imath\omega_2)\,\tilde{G}_s(\imath\omega_\nu)\,\tilde{G}_t(\imath\omega_\nu+\imath\omega_3). \tag{58}$$

From the same reasoning than that of Part 4.1, we have:

$$\left\{\frac{1}{b^2}\,\xi^{(123456)}_{ijkluv}(\imath\omega_1,-\imath\omega_1,\imath\omega_2,-\imath\omega_2,\imath\omega_3)\right\}^{*} = \Big\{\{\alpha_{kj}(\imath\omega_1)\,\alpha_{ul}(\imath\omega_2)\,\alpha_{iv}(\imath\omega_3)\}^{\dagger}\Big\}^{*}, \tag{59}$$

where the $\{\cdot\}^{*/\dagger}$ operators are here defined as:

$$\left\{\sum_{mnqrst} f_{mnqrst}\right\}^{*} = \sum_{mnqrst} f_{mnqrst}\,\delta_{mq}\delta_{ms} = \sum_{mnrt} f_{mnmrmt}, \tag{60}$$

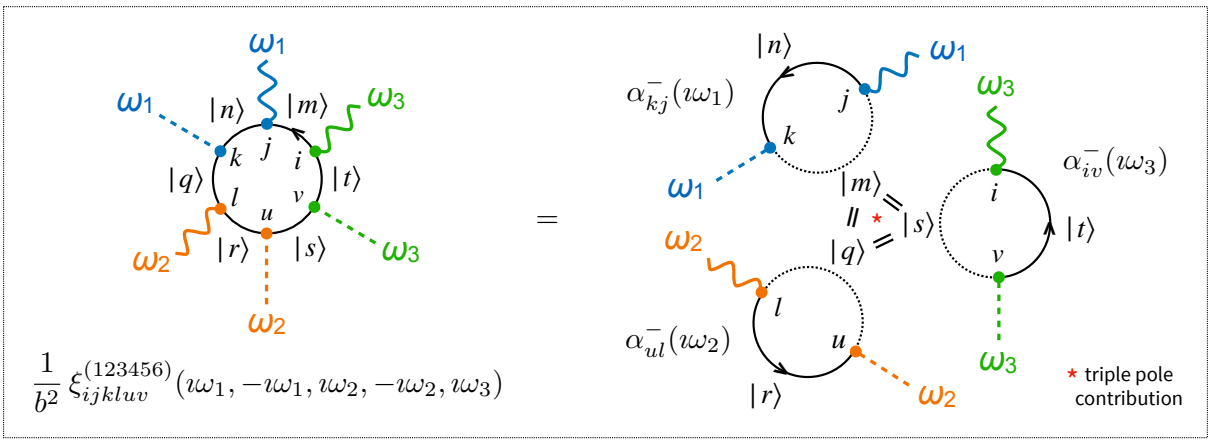

Figure S7: **Factorization of ξ functions.** Diagrammatic representation of equation (63).

and:

$$\left\{\sum_{\nu\lambda\mu} f(\imath\omega_\nu,\imath\omega_\lambda,\imath\omega_\mu)\right\}^\dagger = \sum_{\nu\lambda\mu} f(\imath\omega_\nu,\imath\omega_\lambda,\imath\omega_\mu)\,\delta_{\nu\lambda}\delta_{\nu\mu} = \sum_{\nu} f(\imath\omega_\nu,\imath\omega_\nu,\imath\omega_\nu). \tag{61}$$

The action of these operators is equivalent to extracting the contributions of the triple poles within the ξ function and the product of the three α functions. From Part 2.5, it consists in keeping the terms weighted by the second derivative $\rho''(z)$:

$$\left\{\frac{1}{b^2}\,\xi^{(123456)}_{ijkluv}(\imath\omega_1,-\imath\omega_1,\imath\omega_2,-\imath\omega_2,\imath\omega_3)\right\}^* = \frac{-1}{b^3\hbar^4}\sum_m \rho''(\omega_m)\sum_n \frac{p^k_{mn}p^j_{nm}}{\imath\omega_1-\omega_{nm}}\sum_r \frac{p^u_{mr}p^l_{rm}}{\imath\omega_2-\omega_{rm}}\sum_t \frac{p^i_{mt}p^v_{tm}}{\imath\omega_3-\omega_{tm}}. \tag{62}$$

We retrieve the triply resonant contribution $\alpha^-_{kj}(\imath\omega_1)\,\alpha^-_{ul}(\imath\omega_2)\,\alpha^-_{iv}(\imath\omega_3)$ of the α product, which gives at vanishing temperature:

$$\frac{1}{b^2}\,\xi^{(123456)}_{ijkluv}(\imath\omega_1,-\imath\omega_1,\imath\omega_2,-\imath\omega_2,\imath\omega_3) = \alpha^-_{kj}(\imath\omega_1)\,\alpha^-_{ul}(\imath\omega_2)\,\alpha^-_{iv}(\imath\omega_3). \tag{63}$$

This equation is illustrated by Figure S7.

4.3 Generalization

A generalization of Eq. (38) and (63) is even possible. For any response function $f^{(2n+1)}_{\{i_k\}_{1\leqslant k\leqslant 2n+2}}$ of an odd order $2n+1$ ($n\geqslant 1$), the main term at low temperature is a pole of order $(n+1)$. This leads to the factorization for the dominant term:

$$\frac{1}{b^n}\,f^{(2n+1)}_{\{i_k\}_{1\leqslant k\leqslant 2n+2}}(\{\imath\omega_j,-\imath\omega_j\}_{1\leqslant j\leqslant n},\imath\omega_{n+1}) \;=\; (-1)^n\;\alpha^-_{i_1 i_{2n+2}}(\imath\omega_{n+1})\cdot\prod_{k=1}^{n}\alpha^-_{i_{2k+1}i_{2k}}(\imath\omega_k). \tag{64}$$

This equation is illustrated by Figure S8. In particular:

$$\frac{1}{b}\,\gamma^{(1234)}_{ijkl}(\imath\omega_1,-\imath\omega_1,\imath\omega_2) = \frac{1}{b}\,f^{(3)}_{ijkl}(\imath\omega_1,-\imath\omega_1,\imath\omega_2) = -\,\alpha^-_{il}(\imath\omega_2)\,\alpha^-_{kj}(\imath\omega_1),$$

$$\frac{1}{b^2}\,\xi^{(123456)}_{ijkluv}(\{\imath\omega_j,-\imath\omega_j\}_{1,2},\imath\omega_3) = \frac{1}{b^2}\,f^{(5)}_{ijkluv}(\{\imath\omega_j,-\imath\omega_j\}_{1,2},\imath\omega_3) = \alpha^-_{iv}(\imath\omega_3)\,\alpha^-_{ul}(\imath\omega_2)\,\alpha^-_{kj}(\imath\omega_1).$$

Such factorizations into α functions are only possible when the loops associated to the odd-order response functions are involved in composite diagrams. For any response function of order $(2n+1)$, the coefficient $1/b^n$ has a physical meaning if, and only if, it derives from $n+1$ hidden boson Matsubara frequencies (see Part 2.4). Since $1/b\to 0$ is an infinitesimal parameter, it is expected to be removed through the computation of the total response function associated to the whole composite diagram. Equation (64) is not autonomous, but an intermediate step of the complete calculation of a diagram.

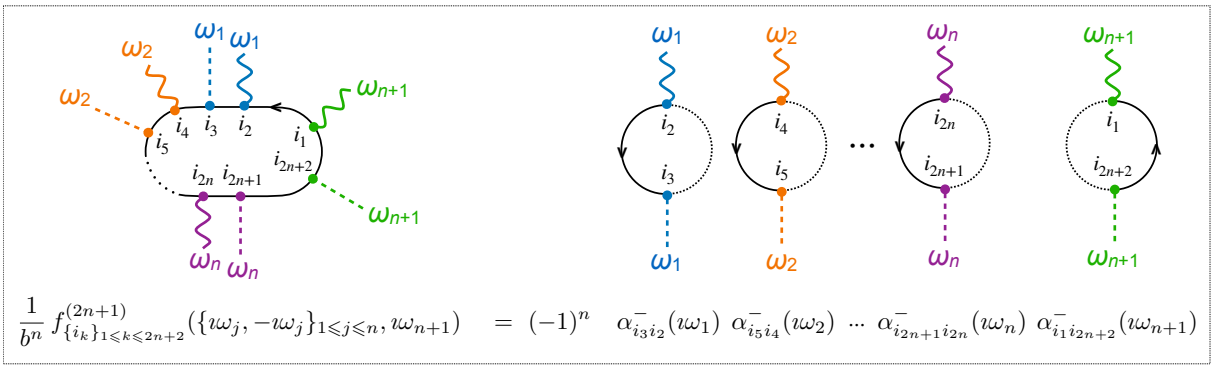

$$\frac{1}{b^n}\,f^{(2n+1)}_{\{i_k\}_{1\leqslant k\leqslant 2n+2}}(\{\imath\omega_j,-\imath\omega_j\}_{1\leqslant j\leqslant n},\imath\omega_{n+1}) \;=\; (-1)^n\;\;\alpha^-_{i_3 i_2}(\imath\omega_1)\;\alpha^-_{i_5 i_4}(\imath\omega_2)\;\cdots\;\alpha^-_{i_{2n+1}i_{2n}}(\imath\omega_n)\;\alpha^-_{i_1 i_{2n+2}}(\imath\omega_{n+1})$$

Figure S8: **Factorization of odd-order response functions.** Diagrammatic representation of Eq. (64).

5 Pairing of diagrams

5.1 One-boson diagrams ($V = 1$)

Figure 1 and Figure S9 show the six 2-loop diagrams made of a single virtual boson linking the nanostructure and the molecule ($V = 1$). Applying the Feynman rules to the first diagram $[1, 1, \downarrow]$, we get:

$$\beta_{ijk}^{[1,1,\downarrow]}(\imath\omega_1, \imath\omega_2) = \sum_{h,l} W_{lh}(\omega_1)\, \frac{1}{b\hbar^2} \sum_{m,n} \sum_{\nu} p_{mn}^{h}\, p_{nm}^{j}\, \tilde{G}_m(\imath\omega_\nu)\, \tilde{G}_n(\imath\omega_\nu + \imath\omega_1) \times \frac{1}{b\hbar^3} \sum_{a,b,c} \sum_{\lambda} \mu_{ac}^{i} \mu_{ba}^{l} \mu_{cb}^{k} \tilde{G}_a(\imath\omega_\lambda)\, \tilde{G}_b(\imath\omega_\lambda + \imath\omega_1)\, \tilde{G}_c(\imath\omega_\lambda + \imath\omega_3). \quad (65)$$

In Part 3.1, we recall the expressions (deduced from the 1-loop diagrams) of the linear polarizability $\alpha_{ij}(\imath\omega)$ (Eq. (26)) and the first hyperpolarizability $\beta_{ijk}^{(123)}(\imath\omega_1, \imath\omega_2)$ (Eq. (31)). Combining these two equations (and applying the analytical continuity $\imath\omega_x \to \omega_x + \imath 0^+$), we straightforwardly deduce (in real frequencies):

$$\beta_{ijk}^{[1,1,\downarrow]}(\omega_1, \omega_2) = -\sum_{h,l} W_{lh}(\omega_1)\; \alpha_{hj}^{\mathrm{N}}(\omega_1)\, \beta_{ilk}^{(123)}(\omega_1, \omega_2), \quad (66)$$

where $\boldsymbol{\alpha}^{\mathrm{N}}(\omega)$ is the polarizability of the nanostructure. By defining matrix $\boldsymbol{Q}(\omega) = -\boldsymbol{W}(\omega) \cdot \boldsymbol{\alpha}^{\mathrm{N}}(\omega)$, we can write:

$$\beta_{ijk}^{[1,1,\downarrow]}(\omega_1, \omega_2) = \sum_{l} Q_{lj}(\omega_1)\, \beta_{ilk}^{(123)}(\omega_1, \omega_2) = \sum_{i'j'k'} \delta_{ii'}\, {}^{t}Q_{jj'}(\omega_1)\, \delta_{kk'}\, \beta_{i'j'k'}^{(123)}(\omega_1, \omega_2). \quad (67)$$

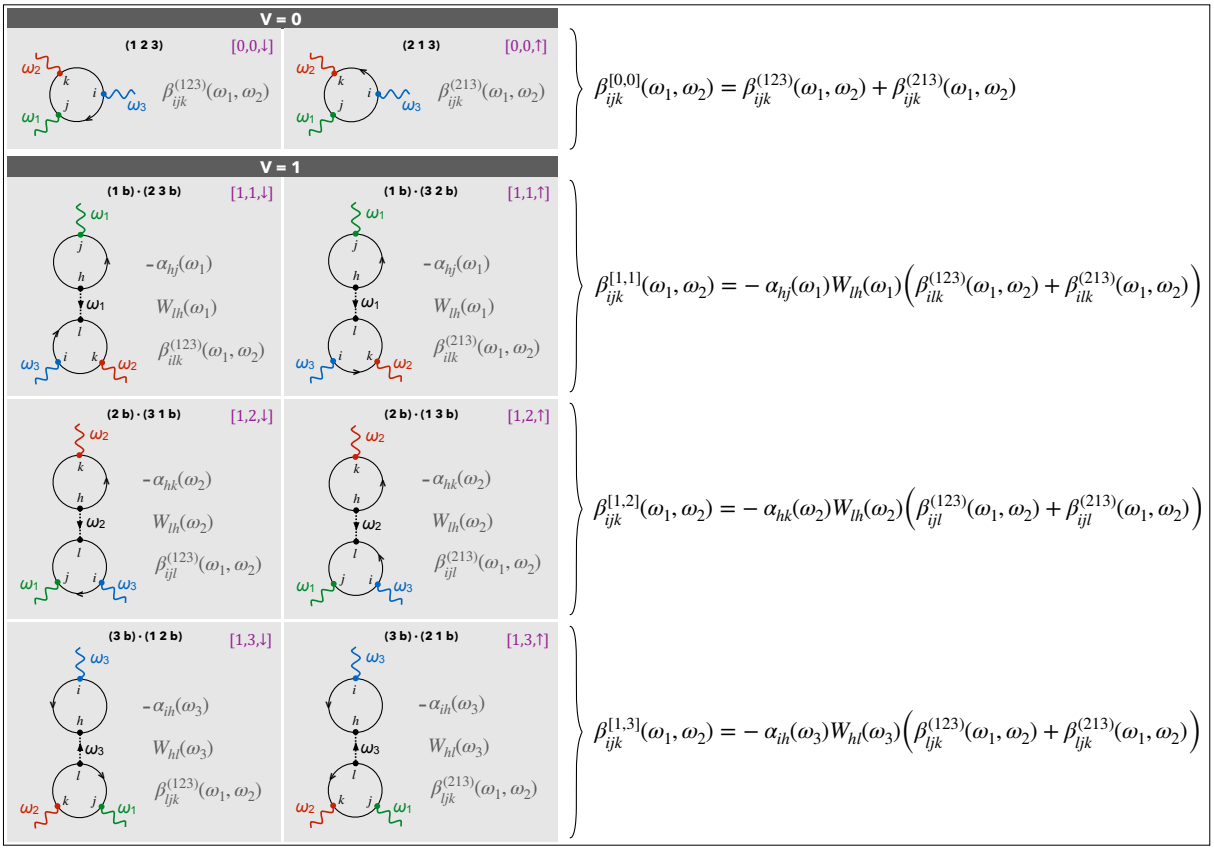

Figure S9: **1-boson diagrams.** Elaboration on the computation of $\beta_{ijk}^{[1,\mathrm{n}_1]}$, $\mathrm{n}_1 = 1, 2, 3$, from the diagrams pictured in Figure 1. We omit the implicit sums over h and l indices.

The same result is obtained from diagram $[1,1,\uparrow]$ with $\beta^{(213)}_{ijk}$, so that we eventually retrieve $\beta^{[0,0]}_{ijk}$:

$$\begin{aligned}\beta^{[1,1]}_{ijk}(\omega_1,\omega_2) &= \beta^{[1,1,\downarrow]}_{ijk}(\omega_1,\omega_2)+\beta^{[1,1,\uparrow]}_{ijk}(\omega_1,\omega_2)\\ &= \sum_{i'j'k'}\delta_{ii'}\,{}^tQ_{jj'}(\omega_1)\,\delta_{kk'}\,\left(\beta^{(123)}_{i'j'k'}(\omega_1,\omega_2)+\beta^{(213)}_{i'j'k'}(\omega_1,\omega_2)\right)\\ &= \sum_{i'j'k'}\delta_{ii'}\,{}^tQ_{jj'}(\omega_1)\,\delta_{kk'}\,\beta^{[0,0]}_{i'j'k'}(\omega_1,\omega_2). \end{aligned} \tag{68}$$

With the same method applied to the diagram $[1,3,\uparrow]$, we find:

$$\begin{aligned}\beta^{[1,3,\uparrow]}_{ijk}(\imath\omega_1,\imath\omega_2) = \sum_{h,l}W_{hl}(\omega_3)\;\frac{1}{b\hbar^2}\sum_{m,n}\sum_{\nu}p^i_{mn}\,p^h_{nm}\,\tilde{G}_m(\imath\omega_\nu)\,\tilde{G}_n(\imath\omega_\nu+\imath\omega_3)\\ \times\frac{1}{b\hbar^3}\sum_{a,b,c}\sum_{\lambda}\mu^l_{ac}\mu^k_{ba}\mu^j_{cb}\tilde{G}_a(\imath\omega_\lambda)\,\tilde{G}_b(\imath\omega_\lambda+\imath\omega_2)\,\tilde{G}_c(\imath\omega_\lambda+\imath\omega_3).\end{aligned} \tag{69}$$

Given Eqs. (26) and (31), we can replace the sums by the corresponding responses functions $-\alpha^{\mathrm{N}}_{ih}$ (of the nanostructure) and $\beta^{(123)}_{lkj}$ (of the molecule):

$$\beta^{[1,3,\uparrow]}_{ijk}(\imath\omega_1,\imath\omega_2) = \sum_{h,l}W_{hl}(\omega_3)\;\left(-\alpha^{\mathrm{N}}_{ih}(\imath\omega_3)\right)\;\beta^{(123)}_{lkj}(\imath\omega_2,\imath\omega_1). \tag{70}$$

From Eq. (32), we eventually get:

$$\beta^{[1,3,\uparrow]}_{ijk}(\omega_1,\omega_2) = -\sum_{h,l}\alpha^{\mathrm{N}}_{ih}(\omega_3)\,W_{hl}(\omega_3)\,\beta^{(213)}_{ljk}(\omega_1,\omega_2). \tag{71}$$

We introduce matrix $\boldsymbol{P}(\omega)=-\boldsymbol{\alpha}^{\mathrm{N}}(\omega)\cdot\boldsymbol{W}(\omega)$ and write:

$$\beta^{[1,3,\uparrow]}_{ijk}(\omega_1,\omega_2) = \sum_{l}P_{il}(\omega_3)\,\beta^{(213)}_{ljk}(\omega_1,\omega_2) = \sum_{i'j'k'}P_{ii'}(\omega_3)\,\delta_{jj'}\,\delta_{kk'}\,\beta^{(213)}_{i'j'k'}(\omega_1,\omega_2). \tag{72}$$

By adding the contributions of the six diagrams of Figure 1, we actually obtain:

$$\beta^{[1,1]}_{ijk}(\omega_1,\omega_2)+\beta^{[1,2]}_{ijk}(\omega_1,\omega_2)+\beta^{[1,3]}_{ijk}(\omega_1,\omega_2) = \sum_{i'j'k'}\Lambda^{(1)}_{ii'jj'kk'}(\omega_1,\omega_2)\,\beta^{[0,0]}_{i'j'k'}, \tag{73}$$

with:

$$\Lambda^{(1)}_{ii'jj'kk'}(\omega_1,\omega_2) = \delta_{ii'}\,{}^tQ_{jj'}(\omega_1)\,\delta_{kk'}+\delta_{ii'}\,\delta_{jj'}\,{}^tQ_{kk'}(\omega_2)+P_{ii'}(\omega_3)\,\delta_{jj'}\,\delta_{kk'}. \tag{74}$$

Figure S9 sums up the method, which is actually based on the factorization of $\beta^{[0,0]}$ by pairing the diagrams drawn on the same row.

5.2 Two-boson diagrams ($V=2$)

Eight of the twenty-four 2-loop diagrams made of two virtual bosons are pictured in Figure 2 and Figure S10. The 16 other analogous diagrams are obtained through the permutation of the three photon frequencies. For $[2,1,\downarrow\uparrow]$, the Feynman rules lead to:

$$\begin{aligned}\beta^{[2,1,\downarrow\uparrow]}_{ijk}(\imath\omega_1,\imath\omega_2) = \frac{1}{b}\sum_{h,l,h',l'}W_{lh}(\omega_2)\,W_{h'l'}(\omega_3)\\ \times\frac{1}{b\hbar^3}\sum_{a,b,c}\sum_{\lambda}\mu^{l'}_{ac}\mu^j_{ba}\mu^l_{cb}\,\tilde{G}_a(\imath\omega_\lambda)\,\tilde{G}_b(\imath\omega_\lambda+\imath\omega_1)\,\tilde{G}_c(\imath\omega_\lambda+\imath\omega_3)\\ \times\frac{1}{b\hbar^4}\sum_{m,n,q,r}\sum_{\nu}p^i_{mr}\,p^k_{nm}\,p^h_{qn}\,p^{h'}_{rq}\,\tilde{G}_m(\imath\omega_\nu)\,\tilde{G}_n(\imath\omega_\nu+\imath\omega_2)\,\tilde{G}_q(\imath\omega_\nu)\,\tilde{G}_r(\imath\omega_\nu+\imath\omega_3).\end{aligned} \tag{75}$$

Using equations (31) and (34) in Part 3.2, we get:

$$\beta^{[2,1,\downarrow\uparrow]}_{ijk}(\imath\omega_1,\imath\omega_2) = \frac{-1}{b}\sum_{h,l,h',l'}W_{lh}(\omega_2)\,W_{h'l'}(\omega_3)\;\gamma^{(1234)}_{ikhh'}(\imath\omega_2,-\imath\omega_2,\imath\omega_3)\;\beta^{(123)}_{l'jl}(\imath\omega_1,\imath\omega_2). \tag{76}$$

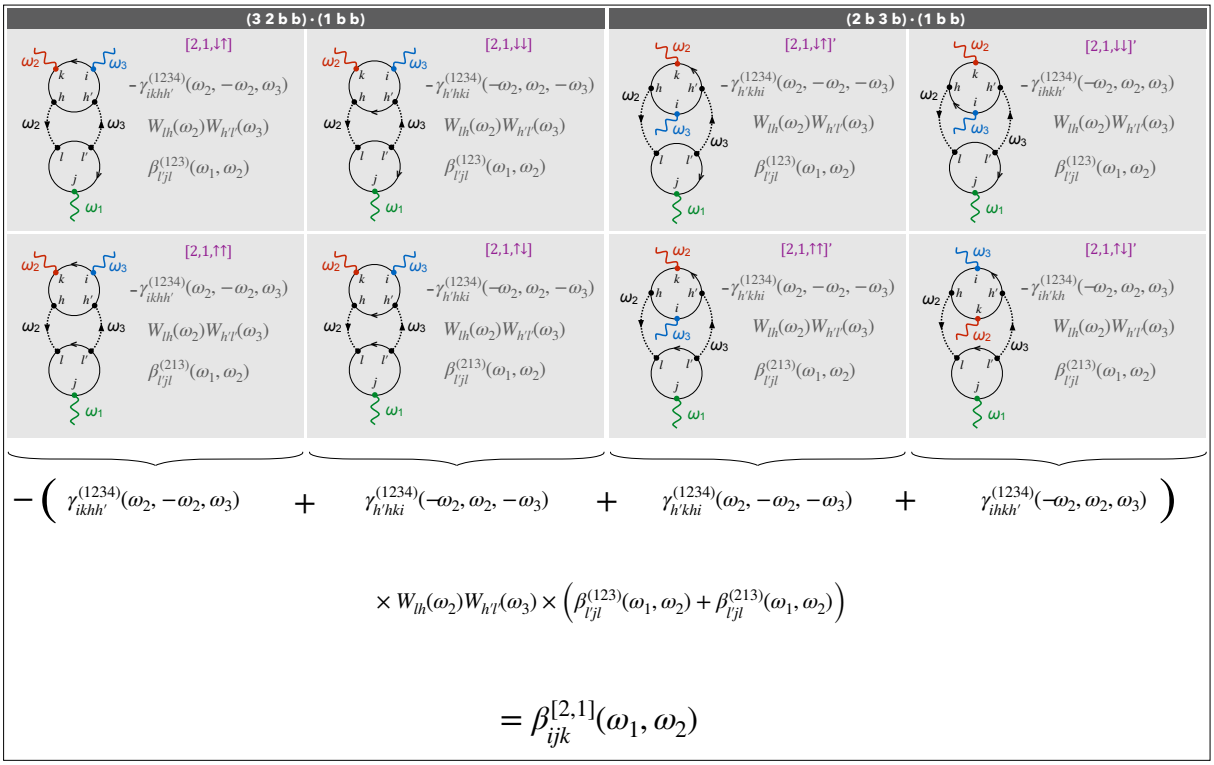

Figure S10: **2-boson diagrams.** Elaboration on the computation of $\beta^{[2,1]}_{ijk}$, from the diagrams pictured in Figure 2. We omit the implicit sums over h, l, h' and l' indices.

In this case, γ is the 3rd-order response function of the nanostructure. Once again, this factorization of $\beta^{(123)}_{l'jl}$ by $W_{lh}(\omega_2)$, $W_{h'l'}(\omega_3)$ and $\gamma^{(1234)}_{ikhh'}(\omega_2,-\omega_2,\omega_3)$ can be directly read on the diagram. By adding the seven other contributions (Figure S10):

$$\beta^{[2,1]}_{ijk}(\imath\omega_1,\imath\omega_2) = \frac{-1}{b}\sum_{h,l,h',l'} W_{lh}(\omega_2)\,W_{h'l'}(\omega_3)\,\Big(\gamma^{(1234)}_{ikhh'}(\imath\omega_2,-\imath\omega_2,\imath\omega_3)+\gamma^{(1234)}_{h'hki}(-\imath\omega_2,\imath\omega_2,-\imath\omega_3) + \gamma^{(1234)}_{h'khi}(\imath\omega_2,-\imath\omega_2,-\imath\omega_3)+\gamma^{(1234)}_{ihkh'}(-\imath\omega_2,\imath\omega_2,\imath\omega_3)\Big)\,\beta^{[0,0]}_{l'jl}(\imath\omega_1,\imath\omega_2). \quad (77)$$

Given that:

$$\begin{aligned}\alpha_{il}(\imath\omega')\,\alpha_{kj}(\imath\omega) &= \alpha^-_{il}(\imath\omega')\,\alpha^-_{kj}(\imath\omega)+\alpha^-_{il}(\imath\omega')\,\alpha^+_{jk}(\imath\omega)+\alpha^+_{li}(\imath\omega')\,\alpha^-_{kj}(\imath\omega)+\alpha^+_{li}(\imath\omega')\,\alpha^+_{jk}(\imath\omega)\\ &= \alpha^-_{il}(\imath\omega')\,\alpha^-_{kj}(\imath\omega)+\alpha^-_{il}(\imath\omega')\,\alpha^-_{jk}(-\imath\omega)+\alpha^-_{li}(-\imath\omega')\,\alpha^-_{kj}(\imath\omega)+\alpha^-_{li}(-\imath\omega')\,\alpha^-_{jk}(-\imath\omega),\end{aligned}$$

it is possible to use Eq. (38) to split each γ function into a product of two α^- functions and to recover the complete product $\alpha_{il}(\imath\omega')\,\alpha_{kj}(\imath\omega)$:

$$\alpha_{il}(\imath\omega')\,\alpha_{kj}(\imath\omega) = \frac{-1}{b}\Big[\gamma^{(1234)}_{ijkl}(\imath\omega,-\imath\omega,\imath\omega')+\gamma^{(1234)}_{ikjl}(-\imath\omega,\imath\omega,\imath\omega') +\gamma^{(1234)}_{ljki}(\imath\omega,-\imath\omega,-\imath\omega')+\gamma^{(1234)}_{lkji}(-\imath\omega,\imath\omega,-\imath\omega')\Big]. \quad (78)$$

Hence, the sum of the four γ functions in equation (77) leads to the product $-\alpha^{\mathrm{N}}_{hk}(\omega_2)\,\alpha^{\mathrm{N}}_{ih'}(\omega_3)$ after application of rule #11 (analytical continuity):

$$\beta^{[2,1]}_{ijk}(\omega_1,\omega_2) = \sum_{h,l,h',l'} W_{lh}(\omega_2)\,W_{h'l'}(\omega_3)\;\alpha^{\mathrm{N}}_{hk}(\omega_2)\,\alpha^{\mathrm{N}}_{ih'}(\omega_3)\;\beta^{[0,0]}_{l'jl}(\omega_1,\omega_2). \quad (79)$$

In other words:

$$\beta^{[2,1]}_{ijk}(\omega_1,\omega_2) = \sum_{i'j'k'} P_{ii'}(\omega_3)\,\delta_{jj'}\,{}^tQ_{kk'}(\omega_2)\;\beta^{[0,0]}_{i'j'k'}(\omega_1,\omega_2). \quad (80)$$

Moreover, in addition to the 8 diagrams of Figure 2, there are 16 analogous diagrams of type $[2,2,\updownarrow\updownarrow]$ and $[2,3,\updownarrow\updownarrow]$, obtained by permutation of the three photon frequencies. Considering these 24 contributions in total, we find on the same principle:

$$\beta_{ijk}^{[2,1]}(\omega_1,\omega_2)+\beta_{ijk}^{[2,2]}(\omega_1,\omega_2)+\beta_{ijk}^{[2,3]}(\omega_1,\omega_2)=\sum_{i'j'k'}\Lambda^{(2)}_{ii'jj'kk'}(\omega_1,\omega_2)\,\beta^{[0,0]}_{i'j'k'}, \tag{81}$$

with:

$$\Lambda^{(2)}_{ii'jj'kk'}(\omega_1,\omega_2)=P_{ii'}(\omega_3)\,\delta_{jj'}\,{}^tQ_{kk'}(\omega_2)+P_{ii'}(\omega_3)\,{}^tQ_{jj'}(\omega_1)\,\delta_{kk'}+\delta_{ii'}\,{}^tQ_{jj'}(\omega_1)\,{}^tQ_{kk'}(\omega_2). \tag{82}$$

5.3 Three-boson diagrams ($V=3$)

Figure 3 and Figure S11 show the 2-loop diagrams built with three virtual bosons. Dealing with the diagram $[3,1,\downarrow\uparrow]$ for instance, the Feynman rules lead to:

$$\beta_{ijk}^{[3,1,\downarrow\uparrow]}(\imath\omega_1,\imath\omega_2)=\frac{1}{b^2}\sum_{h,l,h',l',h'',l''}W_{lh}(\omega_1)\,W_{l'h'}(\omega_2)\,W_{h''l''}(\omega_3)$$

$$\times\frac{1}{b\hbar^6}\sum_{m,n,q,r,s,t}\sum_{\nu}p^i_{mt}\,p^j_{nm}\,p^h_{qn}\,p^k_{rq}\,p^{h'}_{sr}\,p^{h''}_{ts}\,\tilde{G}_m(\imath\omega_\nu)\,\tilde{G}_n(\imath\omega_\nu+\imath\omega_1)\,\tilde{G}_q(\imath\omega_\nu)\,\tilde{G}_r(\imath\omega_\nu+\imath\omega_2)\,\tilde{G}_s(\imath\omega_\nu)\,\tilde{G}_t(\imath\omega_\nu+\imath\omega_3)$$

$$\times\frac{1}{b\hbar^3}\sum_{a,b,c}\sum_{\lambda}\mu^{l''}_{ac}\mu^{l}_{ba}\mu^{l'}_{cb}\tilde{G}_a(\imath\omega_\lambda)\,\tilde{G}_b(\imath\omega_\lambda+\imath\omega_1)\,\tilde{G}_c(\imath\omega_\lambda+\imath\omega_3). \tag{83}$$

As usual, the molecular contribution is identified to $\beta^{(123)}$ according to equation (31). The contribution of the nanostructure loop, corresponding to the sums over (m,n,q,r,s,t) and ν, can be identified to a fifth-order response function $-\xi^{(123456)}_{ijhkh'h''}(\imath\omega_1,-\imath\omega_1,\imath\omega_2,-\imath\omega_2,\imath\omega_3)$ whose diagrammatic definition is given in Section 3.4. In a similar way as for γ functions, Eq. (63) shows that ξ functions can be split into the product of three α^- functions. Examining all the diagrams (Figure S11):

• **Diagrams $[3,0,\downarrow\uparrow]$ and $[3,0,\uparrow\uparrow]$**

$$\begin{aligned}\frac{1}{b^2}\,\xi_{h''jhkh'i}(\imath\omega_1,-\imath\omega_1,\imath\omega_2,-\imath\omega_2,-\imath\omega_3) &= \alpha^-_{h''i}(-\imath\omega_3)\,\alpha^-_{h'k}(\imath\omega_2)\,\alpha^-_{hj}(\imath\omega_1)\\ &= \alpha^+_{h''i}(\imath\omega_3)\,\alpha^-_{h'k}(\imath\omega_2)\,\alpha^-_{hj}(\imath\omega_1).\end{aligned} \tag{84}$$

• **Diagrams $[3,0,\downarrow\downarrow]$ and $[3,0,\uparrow\downarrow]$**

$$\begin{aligned}\frac{1}{b^2}\,\xi_{ih'khjh''}(-\imath\omega_2,\imath\omega_2,-\imath\omega_1,\imath\omega_1,\imath\omega_3) &= \alpha^-_{ih''}(\imath\omega_3)\,\alpha^-_{jh}(-\imath\omega_1)\,\alpha^-_{kh'}(-\imath\omega_2)\\ &= \alpha^-_{ih''}(\imath\omega_3)\,\alpha^+_{kh'}(\imath\omega_2)\,\alpha^+_{jh}(\imath\omega_1).\end{aligned} \tag{85}$$

• **Diagrams $[3,1,\downarrow\uparrow]$ and $[3,1,\uparrow\uparrow]$**

$$\frac{1}{b^2}\,\xi_{ijhkh'h''}(\imath\omega_1,-\imath\omega_1,\imath\omega_2,-\imath\omega_2,\imath\omega_3) = \alpha^-_{ih''}(\imath\omega_3)\,\alpha^-_{h'k}(\imath\omega_2)\,\alpha^-_{hj}(\imath\omega_1). \tag{86}$$

• **Diagrams $[3,1,\downarrow\downarrow]$ and $[3,1,\uparrow\downarrow]$**

$$\begin{aligned}\frac{1}{b^2}\,\xi_{h''h'khji}(-\imath\omega_2,\imath\omega_2,-\imath\omega_1,\imath\omega_1,-\imath\omega_3) &= \alpha^-_{h''i}(-\imath\omega_3)\,\alpha^-_{jh}(-\imath\omega_1)\,\alpha^-_{kh'}(-\imath\omega_2)\\ &= \alpha^+_{h''i}(\imath\omega_3)\,\alpha^+_{kh'}(\imath\omega_2)\,\alpha^+_{jh}(\imath\omega_1).\end{aligned} \tag{87}$$

• **Diagrams $[3,2,\downarrow\uparrow]$ and $[3,2,\uparrow\uparrow]$**

$$\begin{aligned}\frac{1}{b^2}\,\xi_{ijhh'kh''}(\imath\omega_1,-\imath\omega_1,-\imath\omega_2,\imath\omega_2,\imath\omega_3) &= \alpha^-_{ih''}(\imath\omega_3)\,\alpha^-_{kh'}(-\imath\omega_2)\,\alpha^-_{hj}(\imath\omega_1)\\ &= \alpha^-_{ih''}(\imath\omega_3)\,\alpha^+_{kh'}(\imath\omega_2)\,\alpha^-_{hj}(\imath\omega_1).\end{aligned} \tag{88}$$

• **Diagrams $[3,2,\downarrow\downarrow]$ and $[3,2,\uparrow\downarrow]$**

$$\begin{aligned}\frac{1}{b^2}\,\xi_{h''kh'ji}(\imath\omega_2,-\imath\omega_2,-\imath\omega_1,\imath\omega_1,-\imath\omega_3) &= \alpha^-_{h''i}(-\imath\omega_3)\,\alpha^-_{jh}(-\imath\omega_1)\,\alpha^-_{h'k}(\imath\omega_2)\\ &= \alpha^+_{h''i}(\imath\omega_3)\,\alpha^-_{h'k}(\imath\omega_2)\,\alpha^+_{jh}(\imath\omega_1).\end{aligned} \tag{89}$$

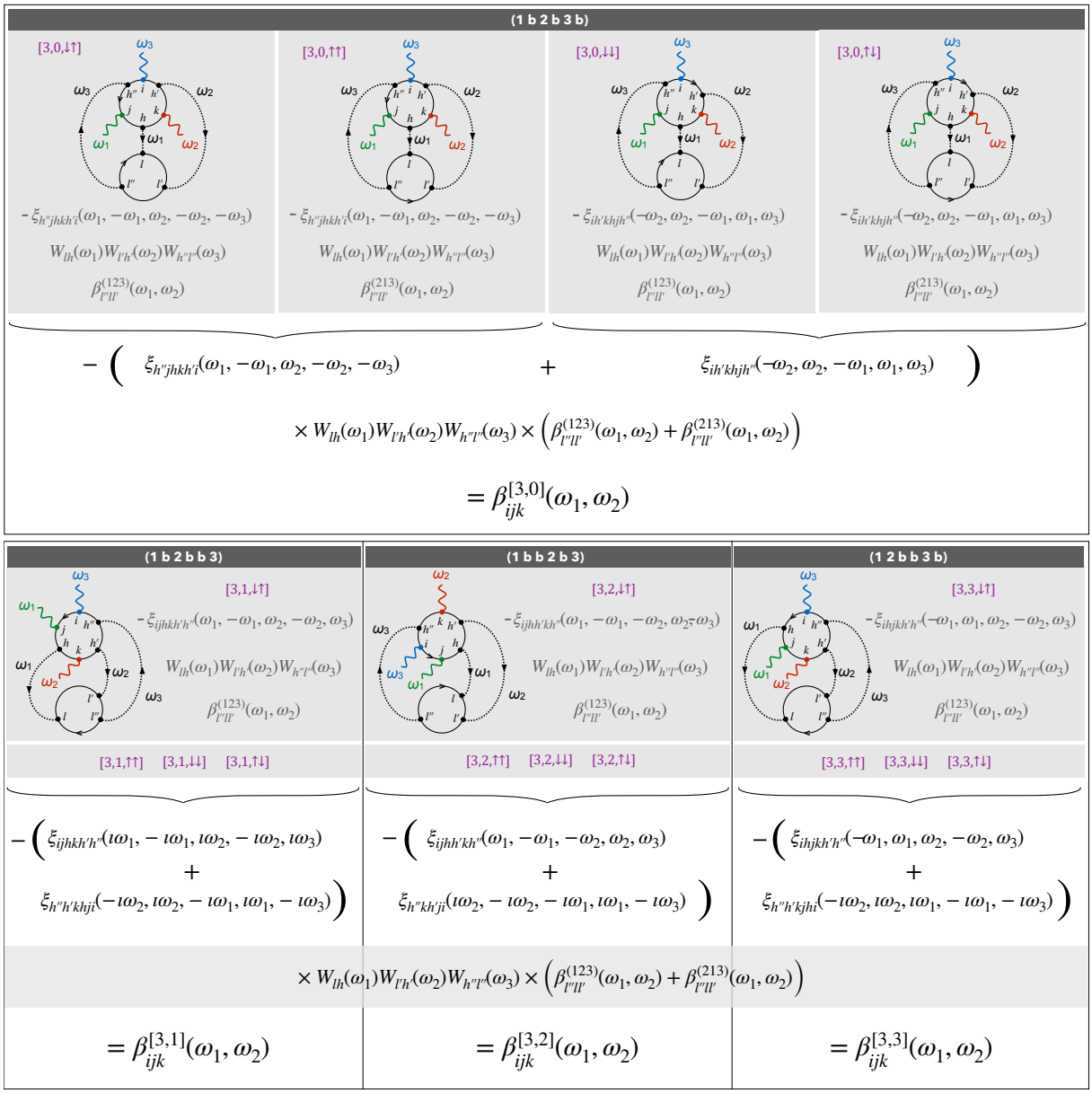

Figure S11: **3-boson diagrams.** Elaboration on the computation of $\beta^{[3,\mathrm{n}_3]}_{ijk}$, $\mathrm{n}_3 = 0,1,2,3$, from the diagrams pictured in Figure 3. We omit the implicit sums over h, l, h', l', h'' and l'' indices.

- **Diagrams $[3,3,\downarrow\uparrow]$ and $[3,3,\uparrow\uparrow]$**

$$\begin{aligned}\frac{1}{b^2}\,\xi_{ihjkh'h''}(-\iota\omega_1,\iota\omega_1,\iota\omega_2,-\iota\omega_2,\iota\omega_3) &= \alpha^-_{ih''}(\iota\omega_3)\,\alpha^-_{h'k}(\iota\omega_2)\,\alpha^-_{jh}(-\iota\omega_1)\\ &= \alpha^-_{ih''}(\iota\omega_3)\,\alpha^-_{h'k}(\iota\omega_2)\,\alpha^+_{jh}(\iota\omega_1).\end{aligned}\tag{90}$$

- **Diagrams $[3,3,\downarrow\downarrow]$ and $[3,3,\uparrow\downarrow]$**

$$\begin{aligned}\frac{1}{b^2}\,\xi_{h''h'kjhi}(-\iota\omega_2,\iota\omega_2,\iota\omega_1,-\iota\omega_1,-\iota\omega_3) &= \alpha^-_{h''i}(-\iota\omega_3)\,\alpha^-_{hj}(\iota\omega_1)\,\alpha^-_{kh'}(-\iota\omega_2)\\ &= \alpha^+_{h''i}(\iota\omega_3)\,\alpha^+_{kh'}(\iota\omega_2)\,\alpha^-_{hj}(\iota\omega_1).\end{aligned}\tag{91}$$

Given that $\alpha_{ij} = \alpha^-_{ij} + \alpha^+_{ji}$, the sum of these 8 terms (Eq. 84-91) is strictly equal to the product of three $\boldsymbol{\alpha}$ components:

$$
\begin{aligned}
\alpha_{ih''}(\imath\omega_3)\,\alpha_{h'k}(\imath\omega_2)\,\alpha_{hj}(\imath\omega_1) &= \alpha^{-}_{ih''}(\imath\omega_3)\,\alpha^{-}_{h'k}(\imath\omega_2)\,\alpha^{-}_{hj}(\imath\omega_1) + \alpha^{-}_{ih''}(\imath\omega_3)\,\alpha^{-}_{h'k}(\imath\omega_2)\,\alpha^{+}_{jh}(\imath\omega_1) \\
&+ \alpha^{-}_{ih''}(\imath\omega_3)\,\alpha^{+}_{kh'}(\imath\omega_2)\,\alpha^{-}_{hj}(\imath\omega_1) + \alpha^{-}_{ih''}(\imath\omega_3)\,\alpha^{+}_{kh'}(\imath\omega_2)\,\alpha^{+}_{jh}(\imath\omega_1) \\
&+ \alpha^{+}_{h''i}(\imath\omega_3)\,\alpha^{-}_{h'k}(\imath\omega_2)\,\alpha^{-}_{hj}(\imath\omega_1) + \alpha^{+}_{h''i}(\imath\omega_3)\,\alpha^{-}_{h'k}(\imath\omega_2)\,\alpha^{+}_{jh}(\imath\omega_1) \\
&+ \alpha^{+}_{h''i}(\imath\omega_3)\,\alpha^{+}_{kh'}(\imath\omega_2)\,\alpha^{-}_{hj}(\imath\omega_1) + \alpha^{+}_{h''i}(\imath\omega_3)\,\alpha^{+}_{kh'}(\imath\omega_2)\,\alpha^{+}_{jh}(\imath\omega_1).
\end{aligned}
$$

The sum of these 8 terms, from Eq. (84) to (91), can be factorized by:

$$
W_{lh}(\omega_1)\,W_{l'h'}(\omega_2)\,W_{h''l''}(\omega_3)\left(\beta^{(123)}_{l''ll'}(\imath\omega_1,\imath\omega_2)+\beta^{(213)}_{l''ll'}(\imath\omega_1,\imath\omega_2)\right), \tag{92}
$$

as shown in Figure S11. After application of rule #11 (analytical continuity), the contributions of these 16 diagrams read:

$$
\begin{aligned}
&\beta^{[3,0]}_{ijk}(\omega_1,\omega_2)+\beta^{[3,1]}_{ijk}(\omega_1,\omega_2)+\beta^{[3,2]}_{ijk}(\omega_1,\omega_2)+\beta^{[3,3]}_{ijk}(\omega_1,\omega_2) \\
&= -\sum_{l,l',l''}\sum_{h,h',h''}\alpha_{ih''}(\omega_3)\alpha_{h'k}(\omega_2)\alpha_{hj}(\omega_1)\cdot W_{lh}(\omega_1)W_{l'h'}(\omega_2)W_{h''l''}(\omega_3)\cdot\beta^{[0,0]}_{l''ll'}(\omega_1,\omega_2) \\
&= \sum_{l,l',l''} P_{il''}(\omega_3)\,Q_{l'k}(\omega_2)\,Q_{lj}(\omega_1)\cdot\beta^{[0,0]}_{l''ll'}(\omega_1,\omega_2) \\
&= \sum_{i'j'k'}\Lambda^{(3)}_{ii'jj'kk'}(\omega_1,\omega_2)\,\beta^{[0,0]}_{i'j'k'},
\end{aligned} \tag{93}
$$

with:

$$
\Lambda^{(3)}_{ii'jj'kk'}(\omega_1,\omega_2) = P_{ii'}(\omega_3)\,{}^tQ_{jj'}(\omega_1)\,{}^tQ_{kk'}(\omega_2). \tag{94}
$$

References

[1] Thomas Noblet, Bertrand Busson, and Christophe Humbert. Diagrammatic theory of linear and nonlinear optics for composite systems. *Phys. Rev. A*, 104:063504, 2021.